Author(s)	Eyler, Michael E.
Title	Polarimetric imaging for the detection of disturbed surfaces
Publisher	Monterey, California. Naval Postgraduate School
Issue Date	2009-06
URL	http://hdl.handle.net/10945/4719

This document was downloaded on May 04, 2015 at 23:02:47

NAVAL POSTGRADUATE SCHOOL

MONTEREY, CALIFORNIA

THESIS

POLARIMETRIC IMAGING FOR THE DETECTION OF DISTURBED SURFACES

by

Michael E. Eyler

June 2009

Thesis Advisor:	R. C. Olsen
Second Reader:	R. Harkins

Approved for public release; distribution is unlimited

THIS PAGE INTENTIONALLY LEFT BLANK

REPORT DOCUMENTATION PAGE		*Form Approved OMB No. 0704-0188*
Public reporting burden for this collection of information is estimated to average 1 hour per response, including the time for reviewing instruction, searching existing data sources, gathering and maintaining the data needed, and completing and reviewing the collection of information. Send comments regarding this burden estimate or any other aspect of this collection of information, including suggestions for reducing this burden, to Washington headquarters Services, Directorate for Information Operations and Reports, 1215 Jefferson Davis Highway, Suite 1204, Arlington, VA 22202-4302, and to the Office of Management and Budget, Paperwork Reduction Project (0704-0188) Washington DC 20503.		
1. AGENCY USE ONLY *(Leave blank)*	**2. REPORT DATE** June 2009	**3. REPORT TYPE AND DATES COVERED** Master's Thesis
4. TITLE AND SUBTITLE Polarimetric Imaging for the Detection of Disturbed Surfaces		**5. FUNDING NUMBERS**
6. AUTHOR(S) Eyler, Michael E. (ENS)		
7. PERFORMING ORGANIZATION NAME(S) AND ADDRESS(ES) Naval Postgraduate School Monterey, CA 93943-5000		**8. PERFORMING ORGANIZATION REPORT NUMBER**
9. SPONSORING /MONITORING AGENCY NAME(S) AND ADDRESS(ES) N/A		**10. SPONSORING/MONITORING AGENCY REPORT NUMBER**
11. SUPPLEMENTARY NOTES The views expressed in this thesis are those of the author and do not reflect the official policy or position of the Department of Defense or the U.S. Government.		
12a. DISTRIBUTION / AVAILABILITY STATEMENT Approved for public release; distribution is unlimited		**12b. DISTRIBUTION CODE**

13. ABSTRACT (maximum 200 words)

This work tested the ability of the fast time-division SALSA polarimetric camera of Bossa Nova Technologies, Ltd. to distinguish disturbed from undisturbed surfaces. Earth and asphalt were imaged, and the data was processed using standard ENVI™ software. The polarization signature of the disturbed earth was not strong, even when processing was employed. The camera was better able to distinguish between the polarization characteristics of patched or disturbed asphalt and the surrounding pavement, particularly when maximum likelihood classification was applied. The current results indicate that the camera needs to be systematically tested for sensitivity to roughness scale and soil type and that the asphalt results need to be further verified.

14. SUBJECT TERMS Polarimetric imaging, polarimetric camera, improvised explosive devices			**15. NUMBER OF PAGES** 77
			16. PRICE CODE
17. SECURITY CLASSIFICATION OF REPORT Unclassified	**18. SECURITY CLASSIFICATION OF THIS PAGE** Unclassified	**19. SECURITY CLASSIFICATION OF ABSTRACT** Unclassified	**20. LIMITATION OF ABSTRACT** UU

NSN 7540-01-280-5500

Standard Form 298 (Rev. 2-89)
Prescribed by ANSI Std. 239-18

THIS PAGE INTENTIONALLY LEFT BLANK

**POLARIMETRIC IMAGING FOR THE
DETECTION OF DISTURBED SURFACES**

Michael E. Eyler
Ensign, United States Navy
B.S., United States Naval Academy, 2008

Submitted in partial fulfillment of the
requirements for the degree of

MASTER OF SCIENCE IN APPLIED PHYSICS

from the

**NAVAL POSTGRADUATE SCHOOL
June 2009**

Author: Michael Eyler

Approved by: R. C. Olsen
                 Thesis Advisor

                 R. Harkins
                 Second Reader

                 James Luscombe
                 Chairman, Department of Physics

iii

THIS PAGE INTENTIONALLY LEFT BLANK

ABSTRACT

This work tested the ability of the fast time-division SALSA polarimetric camera of Bossa Nova Technologies, Ltd. to distinguish disturbed from undisturbed surfaces. Earth and asphalt were imaged, and the data was processed using standard ENVI™ software. The polarization signature of the disturbed earth was not strong, even when processing was employed. The camera was better able to distinguish between the polarization characteristics of patched or disturbed asphalt and the surrounding pavement, particularly when maximum likelihood classification was applied. The current results indicate that the camera needs to be systematically tested for sensitivity to roughness scale and soil type and that the asphalt results need to be further verified.

THIS PAGE INTENTIONALLY LEFT BLANK

TABLE OF CONTENTS

THIS PAGE INTENTIONALLY LEFT BLANK

LIST OF FIGURES

THIS PAGE INTENTIONALLY LEFT BLANK

ACKNOWLEDGMENTS

THIS PAGE INTENTIONALLY LEFT BLANK

I.   INTRODUCTION

Polarimetric imaging is a technique that employs cameras with polarizing filters to probe the fine surface texture in the scene being imaged. Because of their sensitivity to roughness, polarimetric imagers may be able to detect the disturbances left by the burial of objects. If so, they may prove useful in the fight against buried improvised explosive devices (IEDs).

The Joint Improvised Explosive Device Defeat Organization (JIEDDO) has described the IED as a "weapon of strategic influence"—a cheap, simple, asymmetric means of inflicting casualties to break the political will of a better-equipped opponent (JIEDDO, 2009, Objectives section, para. 4). IEDs have been a major factor in Operations Enduring Freedom and Iraqi Freedom. The independent web site iCasualties.org (2009) reports that as of 18 May 2009, IEDs in Iraq alone have killed 1,828 coalition force members, wounded many others, and harmed thousands of civilians. Even outside Iraq and Afghanistan, IEDs are a persistent and widespread problem. Hundreds of attacks occur each month, particularly in Colombia, India, Indonesia, Pakistan, the Philippines, Chechnya, and Sri Lanka (Zorpette, 2008).

JIEDDO's counter-IED approach recognizes two major facts. First, IEDs and IED casualties cannot be eliminated entirely, so the best course is to minimize their effectiveness and hence their strategic influence. Second, there is no cure-all solution, so an effective response must incorporate diverse elements including armor, intelligence, proper tactics, law enforcement techniques, gaining local trust, and a whole toolbox of technical assets. These combined efforts aim to defeat both the devices themselves and the networks that build them (Zorpette, 2008).

In order to improve technology-based IED-defeating capabilities, JIEDDO has pledged to maintain a network of partnerships with the science and technology communities (JIEDDO, 2009, Objectives section, para. 2). In this technical arena, however, the IED users have a major advantage: expensive, sophisticated, laboriously developed IED countermeasures can often be defeated using cheap solutions that can be

fielded very quickly (Zorpette, 2008). Because of this imbalance, IED countermeasures are particularly desirable if they are effective, low-cost, and robust.

Polarimetric imagers are one possibility that meets those criteria. Current counter-IED remote sensing techniques include thermal and (hyper)spectral imaging along with radio-frequency and electric or magnetic field detection (Zorpette, 2008), but polarimetric imaging is a largely unexplored possibility. With their sensitivity to roughness, polarimetric imagers may be able to detect the tell-tale disturbed earth left by the burial of explosive devices or their often-associated wires and triggers. Such disturbances are a known visual cue that has been incorporated into soldiers' counter-IED training (Zorpette, 2008). Polarimetric cameras could augment these visual searches, and they may also prove useful for remotely detecting asphalt disturbances and patching.

Besides these particular applications, polarimetry is of general importance to the remote sensing community. In imagery, polarimetric information is mostly uncorrelated with spectral or intensity information; whereas spectral content reveals material composition, polarization informs about "surface features, shape, shading, and roughness" (Tyo et al., 2006). Remote sensing of polarization at optical wavelengths has only begun to be explored since the advent of imaging polarimetry in the 1970s (Egan et al., 1991; Tyo et al., 2006). Polarimetric imaging thus has high potential for augmenting remote sensing capabilities in general and disturbed-surface detection in particular.

This research aimed to evaluate the disturbed-surface detection potential of a simple polarimetric camera designed and built by Bossa Nova Technologies, Ltd. In particular, the purpose was to determine whether the difference between disturbed and undisturbed surfaces is visually obvious in polarization imagery. If it was not found to be so, the further task was to explore some tools that could help to pick out a disturbed-surface polarimetric signature. To these ends, images of both disturbed earth and patched asphalt were taken and analyzed using ENVI™ imaging processing software. The results form the basis for further work and clarify some of the challenges involved in making the camera a useful military system. In addition, the images provide polarimetric data for analysis that can be of general interest to the remote sensing community.

II.   BACKGROUND

A.   GENERAL HISTORY

Light can be characterized by its intensity, spectrum, coherence, and polarization state (Tyo et al., 2006). European investigators began recording their observations of optical polarization in the 17th century. The phenomenon was first quantitatively analyzed by French military engineer and physicist Étienne-Louis Malus, who announced his findings in the bulletin of the Société d'Arcueil (Malus, 1809). Several years later, Sir David Brewster successfully formulated a relation between the polarization of reflected light and the refractive index of the reflecting material, a step which Malus had been unable to accomplish due to the poor quality of glass available to him for use in his experiments (Brewster, 1815). These discoveries were further amplified by the work of Augustin-Jean Fresnel and George G. Stokes, among others. Their combined work contributed to a developing wave theory of light (Wolinski, 2003).

Stokes' work is particularly important for quantifying polarization. He introduced the Stokes parameters, four measurable quantities that give the polarization content of a light beam:

> When any number of independent polarized streams, of given refrangibility, are mixed together, the nature of the mixture is completely determined by the values of four constants, which are certain functions of the intensities of the streams, and of the azimuths and eccentricities of the ellipses by which they are respectively characterized; so that any two groups of polarized streams which furnish the same values for each of these four constants is optically equivalent. (Stokes, 1852)

The Stokes formulation is especially useful because it describes light that is mixed in content (i.e., partially polarized), which is very often encountered in nature.

While remote sensing has long utilized intensity and spectral imagery, it was not until recent decades that the community began giving increasing attention to optical polarization (e.g., Egan & Hallock, 1966; Talmadge & Curran, 1986; Egan et al., 1991). Early efforts focused on simply detecting polarization state without forming images of the target. By the 1970s, technological advances permitted the measurement of

polarization state across a scene, and imaging polarimetry became possible (Egan et al., 1991; Tyo et al., 2006). Fig. 1 shows the significant potential for target detection using imaging polarimetry, showing a visible-wavelength color image of two trucks in the shade, along with long-wave IR intensity and polarization images. The advantage in polarization is clear. Polarimetry and rough surfaces – the application with which this thesis is concerned—will be discussed in Section C of this chapter; the following section gives some necessary theoretical background.
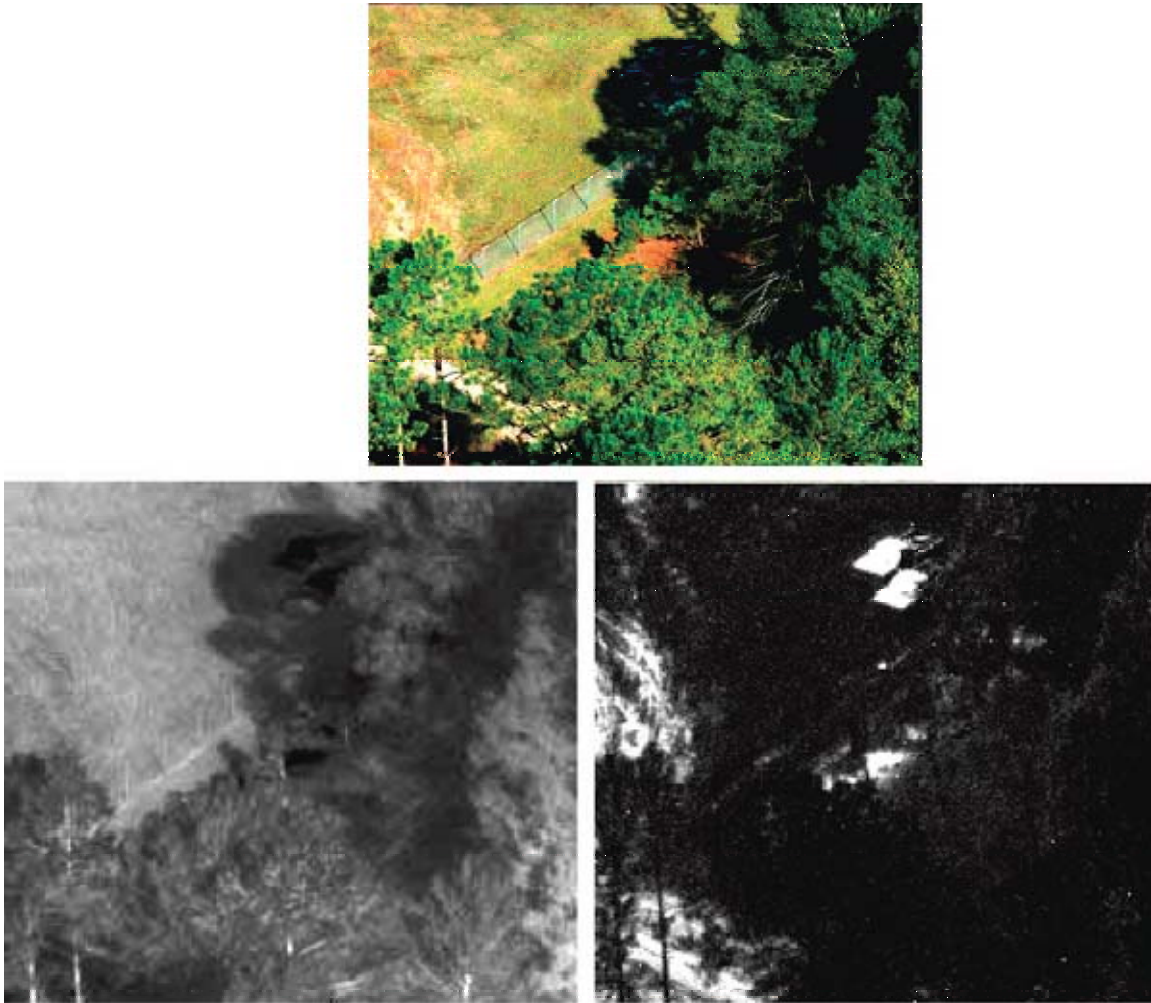

Figure 1.   Polarimetric Target Detection (from Tyo et al., 2006).

B.   POLARIZATION THEORY

1.   Quantifying Polarization

Maxwell's equations show that the electric and magnetic field components of electromagnetic waves are always orthogonal to one another and to the direction of propagation, so it is possible to describe the direction of oscillation—the polarization—using only one component. The electric field component for a wave propagating in the z-direction is given by

$$\overset{\text{\tiny w}}{E} = \hat{x}E_x \cos(kz - vt + \varphi_1(r,t)) + \hat{y}E_y \cos(kz - vt + \varphi_2(r,t)) ,$$

where the terms φ_1 and φ_2 account for the possibility of a location—and/or time-dependent difference in phase between the x and y components of the electric field (Andreou & Kalayjian, 2002). Due to this phase difference, the tip of the electric field vector traces a helical path about the z-axis as the wave propagates.

If the phase difference $\varphi_2 - \varphi_1$ is constant, then the projection of this helical path on the x-y plane will always be ellipse whose orientation and ellipticity depend on the magnitudes and phases of the x and y components. Two special cases of elliptical polarization are circular polarization, where $E_x = E_y$ and $\varphi_2 - \varphi_1 = \pi/2$, and linear polarization, where $\varphi_2 - \varphi_1 = 0$. If there is no fixed relationship between the two phases, the electric field vector direction will vary randomly (while remaining perpendicular to the z-axis), resulting in "natural" or unpolarized light. Fig. 2 gives head-on views from left to right of the circular, linear, and unpolarized cases (Andreou & Kalayjian, 2002).

As noted earlier, light in nature is often partially polarized; i.e., some of the light received from a reflection will be unpolarized and some will be polarized. It is possible to represent monochromatic or near-monochromatic light as the sum of completely unpolarized and completely polarized parts. The degree of polarization P of the wave may then be quantified as the ratio of the intensities of these the polarized parts to the total received intensity: $P = I_{pol}/I_{tot}$ (Born & Wolf 1999).
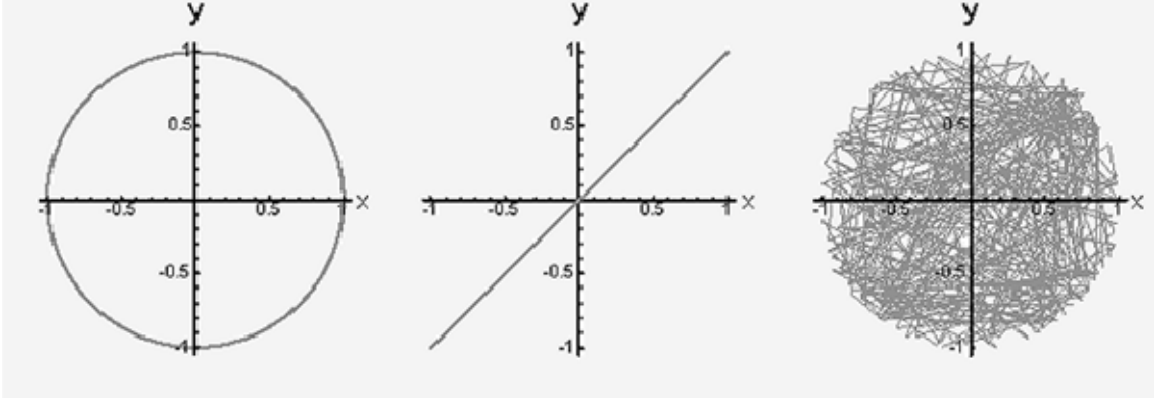
Figure 2.   Possible Polarization States (from Andreou and Kalayjian, 2002).

To completely describe and work with polarization state, it is most convenient to collect the Stokes parameters into a vector $\overline{S}$. The parameters are commonly designated *I*, *Q*, *U*, and *V*, or alternatively, s_0, s_1, s_2, s_3. Given the measured light intensities $I(\theta, \varepsilon)$, where θ represents the angle of polarization with respect to the horizontal *x*-axis and $\varepsilon = \varphi_2 - \varphi_1$, the Stokes vector is

$$\overline{S} = \begin{bmatrix} I \\ Q \\ U \\ V \end{bmatrix} = \begin{bmatrix} s_0 \\ s_1 \\ s_2 \\ s_3 \end{bmatrix} = \begin{bmatrix} I(0°,0) + I(90°,0) \\ I(0°,0) - I(90°,0) \\ I(45°,0) - I(135°,0) \\ I(0°, \pi/2) - I(135°, \pi/2) \end{bmatrix}.$$

The parameter *I* gives the total intensity. *Q* represents the difference in intensity accepted through polarizers oriented at 0° and 90° with respect to the *x*-axis. *U* has a similar interpretation for the 45° and 135° orientations. *V* represents the difference in circular polarizations in the right-handed and left-handed senses (Born & Wolf, 1999).

In terms of the Stokes parameters, then, the degree of polarization may be written as

$$P = \sqrt{Q^2 + U^2 + V^2}/I .$$

This project is concerned only with linear polarization, so only *I*, *Q*, and *U* are of interest. So, rather than the degree of polarization, the quantity of concern is the degree of *linear* polarization, or DOLP (Tyo et al., 2006):

$$P = \sqrt{Q^2 + U^2}\Big/I \quad .$$

It should be noted that camera maker Bossa Nova Technologies has chosen a slightly different formulation for the Stokes vector, given by (Lefaudeux et al., 2007)

$$\overset{\varpi}{S} = \begin{bmatrix} I \\ Q \\ U \end{bmatrix} = \begin{bmatrix} s_0 \\ s_1 \\ s_2 \end{bmatrix} = \begin{bmatrix} 0.5 & 0.5 & 0.5 & 0.5 \\ 1 & -1 & 0 & 0 \\ 0 & 0 & 1 & -1 \end{bmatrix} \begin{bmatrix} I_{0°} \\ I_{90°} \\ I_{45°} \\ I_{135°} \end{bmatrix} \quad .$$

Here, the parameter I is measured by $I = (I_{0°} + I_{90°} + I_{45°} + I_{135°})/2$, rather than $I = I_{0°} + I_{90°}$, but the end result and the expression for DOLP remain the same. This approach is common in the absence of circular polarization measurements; it enhances the signal-to-ratio for the average intensity I.

The above expressions are consistent with the law of Malus, which governs the intensity of light viewed through a polarizing filter. This relation is

$$I(\theta) = I_0 \cos^2 \theta \quad ,$$

where I_0 is the intensity of the incident light and θ is its angle of polarization relative to the light orientation passed by the filter (Collett 2005).

2.   Causes of Polarization

Light can be polarized upon emission from a polarized source, or it can become polarized by some means as it travels from the source to the observer. Polarized emission is often man-made (e.g., lasers or radio broadcasts), while unpolarized sources – most importantly, the Sun—are much more common in nature (Andreou & Kalayjian, 2002). Even so, the light observed in nature is generally polarized to some degree, having become polarized usually by reflection or scattering from one or more particles or objects on the way to the observer. Each scattering or reflection event can modify the polarization of the light, which generally results in some degree of linear polarization. Circular polarization in nature is comparatively rare (Können, 1985).

Light will scatter in any direction from small particles such as dust or electrons whose sizes are much less than the wavelength of the incident light. Light that is

scattered directly backwards or forwards is not polarized, while light that is scattered at a scattering angle of $\theta = 90°$ is totally linearly polarized. This fact is responsible for the higher linear polarization of the blue light of the sky – which is simply sunlight that has undergone Rayleigh scattering – at an angle of $90°$ from the line of sight to the Sun (Können, 1985).

Scattering stands in contrast to the reflection of light from surfaces, whose irregularities are small relative to the incident wavelength. Such reflection may be termed specular reflection (as opposed to diffuse reflection—see below) or simply reflection. In such cases, the electrons of the surface atoms "cooperate" in such a way as to reflect light in a single highly predictable direction. External reflection from both metallic and non-metallic surfaces yields light polarized parallel to the reflecting surface, and in nature, it occurs not only for surfaces like water or ice, but also for objects such as smooth stones or even grass (Können, 1985).

Fresnel's relations describe specular reflection from a dielectric surface for the cases of light whose electric field oscillations are (a) parallel or (b) perpendicular to the plane of incidence, which is defined as the plane containing the incident beam, reflected beam, and the normal to the surface. For case (a), the amplitude reflectance is given by (Olsen, 2007)

$$r_\perp = \frac{n_2 \cos\theta_1 - n_1 \cos\theta_2}{n_2 \cos\theta_1 + n_1 \cos\theta_2} \quad ,$$

and for case (b), it is given by

$$r_\parallel = \frac{n_1 \cos\theta_1 - n_2 \cos\theta_2}{n_1 \cos\theta_1 + n_2 \cos\theta_2} \quad ,$$

where n_1 and n_2 and θ_1 and θ_2 are the indices of refraction and the angles of incidence and refraction in the first and second media, respectively (Olsen, 2007). These reflectances give the amplitude of the reflected wave relative to the incident wave in each polarization state, so the reflected/incident relative intensity can be calculated from the square of these reflectances. (These reflectances can also be expressed entirely in terms of the incident angle and the refractive indices by the use of Snell's law, but the resulting expressions are much more cumbersome.)

In many natural situations of interest, light is incident from a medium of lower refractive index upon one of higher refractive index (e.g., air to glass). Fig. 3 displays the relative intensity of the reflected beams corresponding to the $r_\parallel$ and $r_\perp$ components for a case where $n_1 = 1$ and $n_2 = 1.5$ and the incident angle is measured relative to the normal at the interface. For most incident angles, the relative intensity of the reflected $r_\parallel$ polarization tends to be much smaller than that of the $r_\perp$ polarization, so specularly reflected light is often highly polarized in the $r_\perp$ direction. (Note that $r_\perp$ polarization corresponds to polarization *parallel* to the reflecting surface, and $r_\parallel$ polarization corresponds to polarization *perpendicular* to the reflecting surface, since the plane of incidence and the reflecting surface are perpendicular to one another.) The elimination of horizontally-polarized "glare" from specular reflectors such as bodies of water or horizontal vehicle surfaces is the principle behind polarized sunglasses, which filter out the horizontally polarized component of the reflected light.
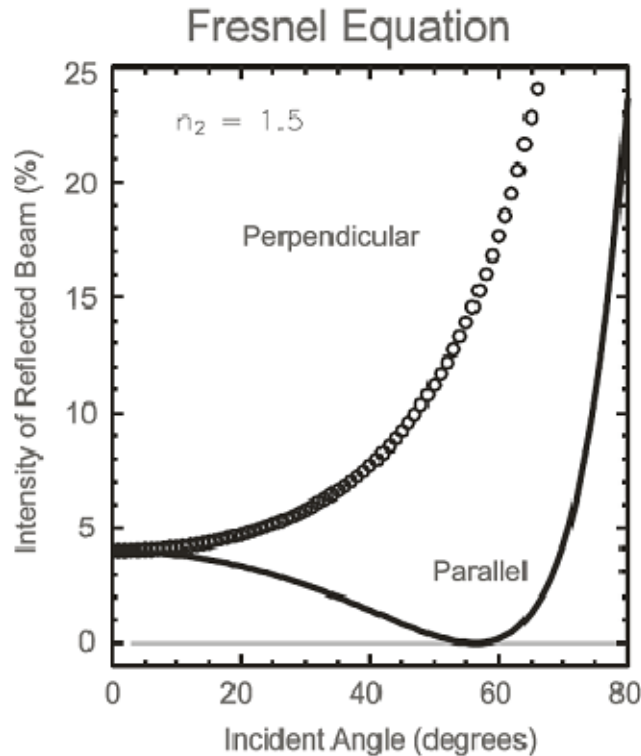

Figure 3.   Reflected Component Relative Intensities (from Olsen, 2007).

9

Reflection from a surface may also be diffuse, or random in direction. Such reflection occurs when the wavelength of the incident light is small relative to surface irregularities so that the surface is effectively "rough" (Olsen, 2007). Diffuse reflection may also be termed scattering, since it can be considered as scattering from many small particles (Können 1985). A surface is considered rough if it meets Rayleigh's criterion of $h > \lambda/(8\cos\theta)$, where h is the height of surface irregularities and λ and θ are the wavelength and angle of incidence of the light (with respect to the normal to the surface), respectively. Another definition allows an intermediate case between rough and smooth of $\lambda/(25\cos\theta) < h < \lambda/(8\cos\theta)$, so that the surface is considered smooth only for $h \leq 25\cos\theta$ (Rees, 2001). Fig. 4 shows the simpler ($\lambda/8$) roughness criterion as a function of θ for green light. It is apparent that most surfaces are rough ($h > \sim 0.1\,\mu\text{m}$) at most angles. Out of man-made materials, mirrors and metals are the types of surfaces that would be considered smooth. On the other hand, even for relatively rough materials, incidence angles very close to the horizontal will reflect at least somewhat specularly.
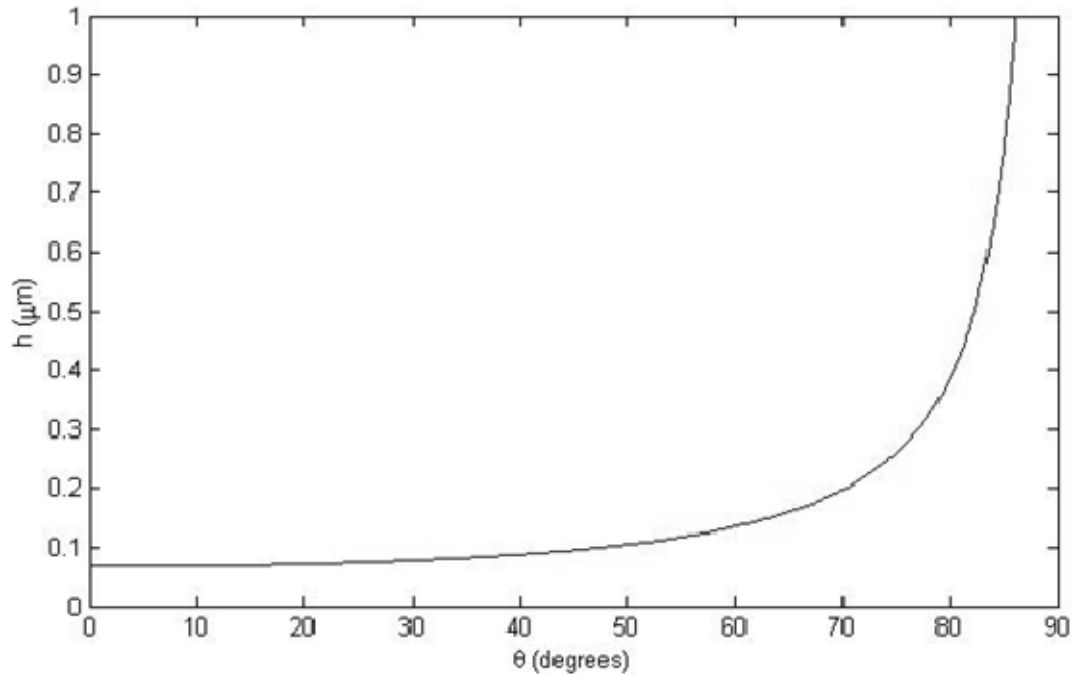

Figure 4.   Rayleigh Roughness Criterion as a Function of Incident Angle.
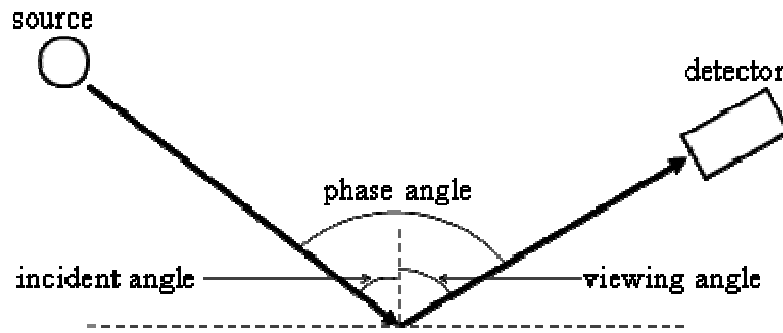
Figure 5.   Definition of Geometrical Terms (after Egan & Hallock, 1966).

C.   POLARIZATION AND SURFACE ROUGHNESS

Light reflected from rough surfaces is usually less polarized than for smooth surfaces (Können, 1985). Although it is obvious from Rayleigh's criterion that most surfaces in nature are optically rough, it may be supposed that polarimetry can distinguish between varying degrees of roughness due to the effect of multiple reflections from irregularities at the surface. It is therefore to be expected that polarization decreases with increasing surface roughness.

Observations have confirmed that reflected polarization varies with surface roughness (along with related factors, such as albedo). The 1960s saw several pioneering studies of polarization by soil surfaces. Egan and Hallock (1966) used a non-imaging photometer polarimeter to examine the relationship between percent polarization and phase and viewing angle for various natural surfaces, noting characteristic features of the percent polarization including maximum and minimum percent polarization, the ratio between them, the phase angles of where they occurred, and the rise in polarization with phase angle (Fig. 5 defines geometrical terms). A viewing angle of 60° was used throughout. The study found that, in general, the maximum polarization at a phase angle of 120° differs with material and spectral band. The authors note that interpreting polarization characteristics is difficult due to the many surface effects involved – reflecting, shadowing, diffraction, and sometimes refraction, so that experimental observations lead theoretical predictions.

11

Egan et al., (1968) concluded from polarization data in several spectral bands that in general, depolarization by soils is greater for smaller particles, rougher or more porous surfaces, and lower moisture content. Their study used a He-Ne laser and scattering materials including basalt, limonite, Haleakala volcanic ash, wet and dry sand, gravel, silt, and foliage. They tested viewing angles of 0° and 60°, incident polarizations parallel and perpendicular to the scattering surface, and various phase angles. The incident radiation was 100% plane polarized, so they defined the depolarization as

$$D = 100 - P,$$

where P is the degree of polarization defined earlier.

Particle size effects were tested using the Haleakala ash, and the trend towards greater depolarization with smaller particles was true for both viewing angles and incident polarizations. Egan et al. (1968) attributed this to the "increased effectiveness of multiple scattering" with decreasing particle size, since the "cascaded" effects of reflection, diffraction, and refraction in the surface particles led to greater randomness in the polarization of the light that finally exited the surface. Fig. 6 shows this trend.

The results of Egan et al., (1968) concerning surface porosity and irregularity were drawn from their study of basalt powder. They sieved and lightly compacted two samples to achieve different porosities and found that the more porous sample produced greater depolarization at both incident polarizations and viewing angles, as shown in Fig. 7. This result suggests that more irregular surfaces cause greater depolarization of incident light.

Notably, this result is consistent with the conclusions of lunar surface studies (see Dollfus, 1998), which find that polarization by lunar impact regoliths (loose material lying over bedrock) is affected slightly by the degree of compaction of the surface layer. Geake et al., (1970) show the modification of the polarization curve by the compaction effect; see Fig. 8. Polarization P is plotted as a function of phase angle V. Significantly, these studies find that the degree of polarization is sensitive to surface roughness only on the scale of millimeters and smaller; larger-scale surface roughness has no effect. Albedo also has a large effect.
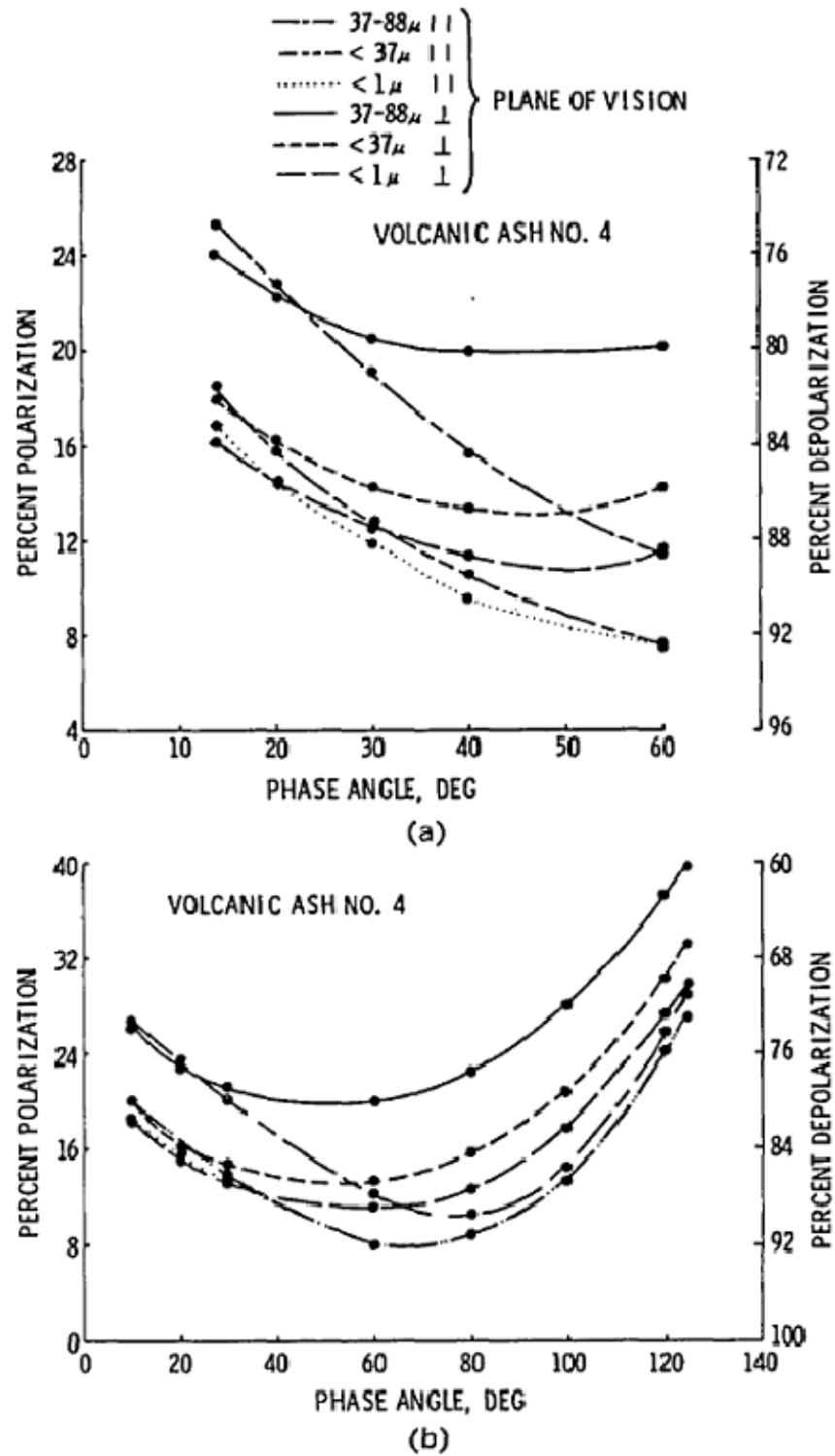
Figure 6.   Haleakala Ash Depolarization for (a) 0° Viewing Angle and (b) 60° Viewing Angle (from Egan et al., 1968).
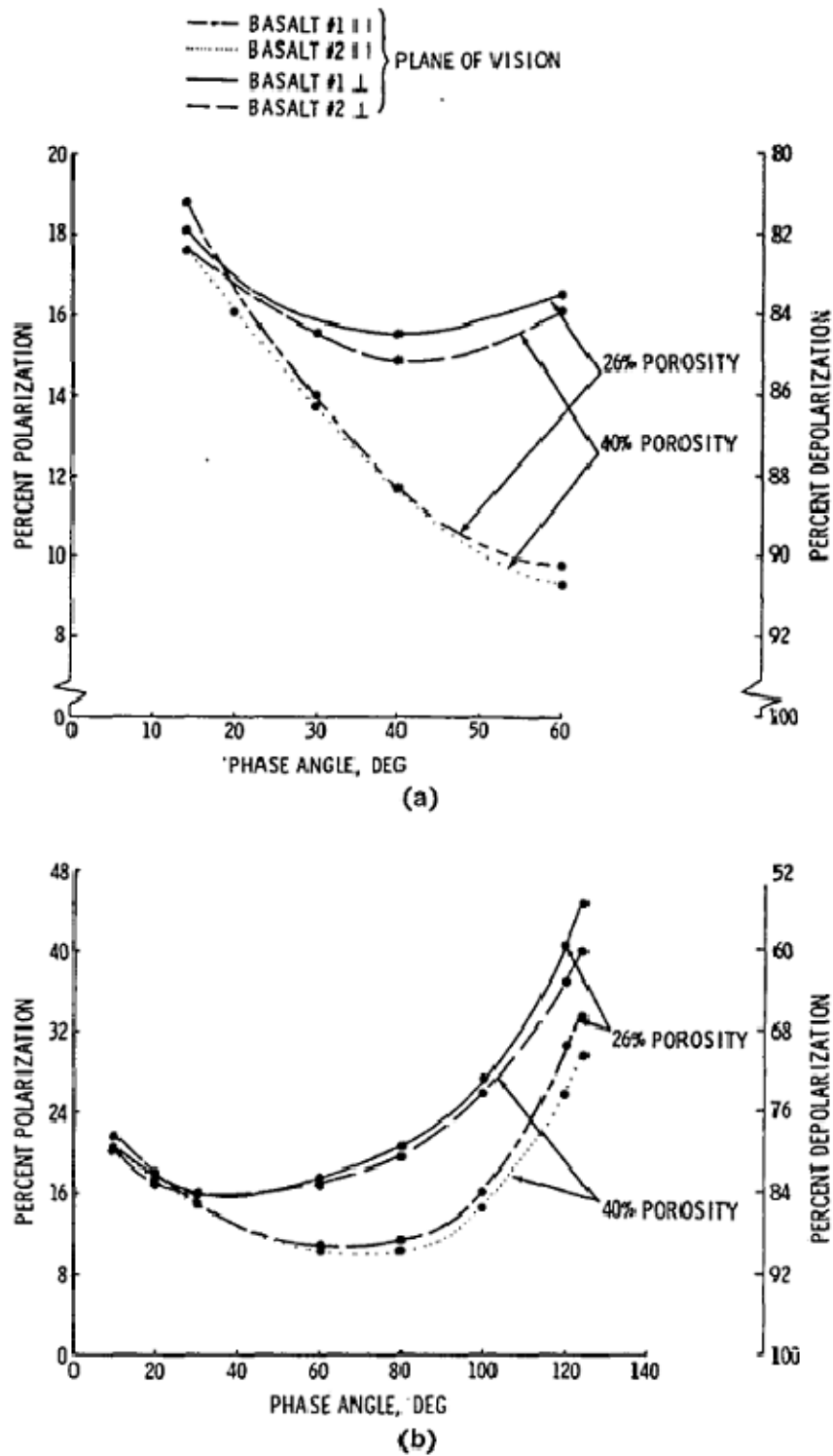
Figure 7.   Basalt Depolarization at (a) 0° Viewing Angle and (b) 60° Viewing Angle
(from Egan et al., 1968).

14
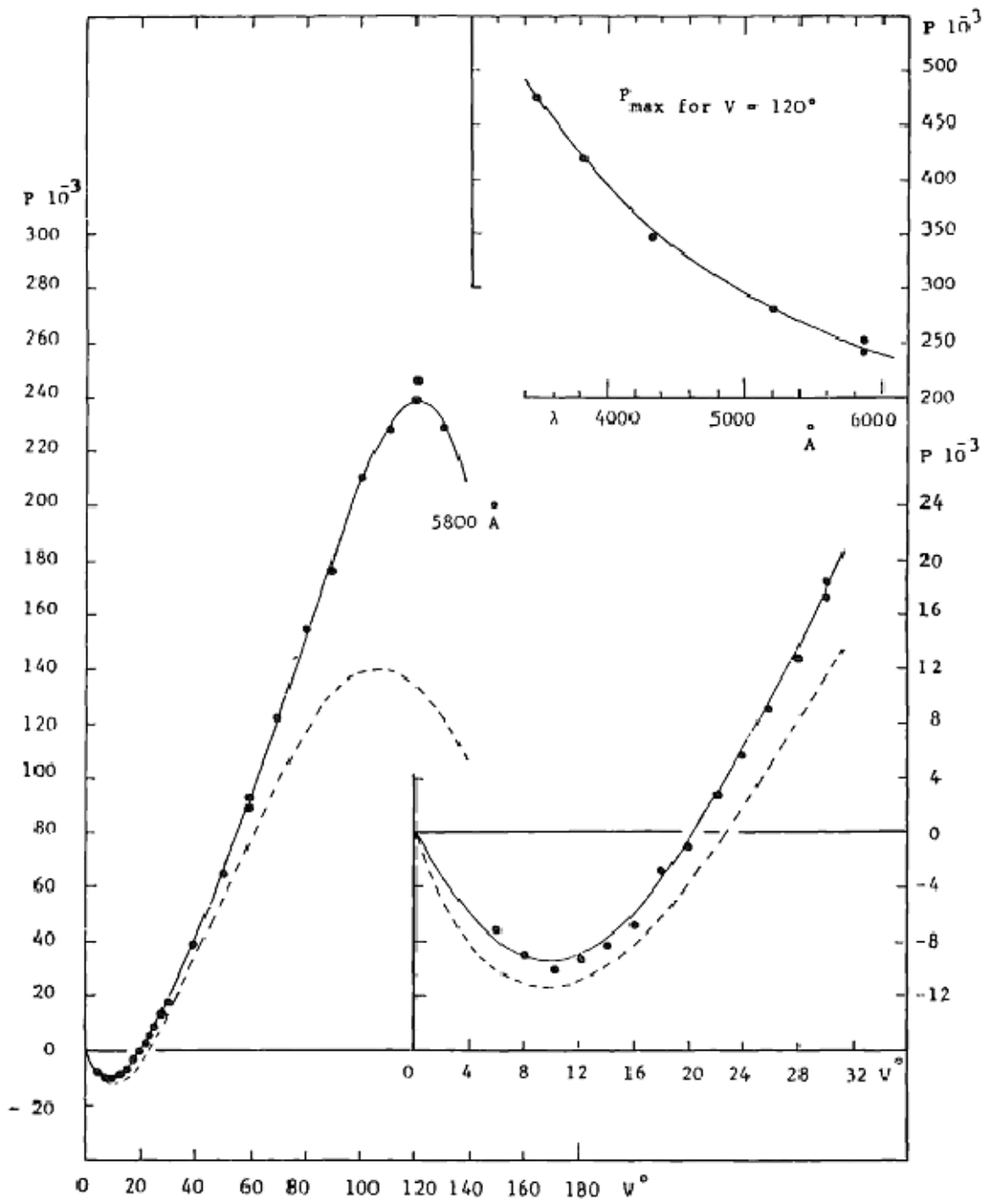
Figure 8.   Lunar Fine Polarization Characteristics for Flattened (solid lines) and
Roughened (dashed lines) Samples (from Geake et al., 1970).

15

This study was followed by Egan and Hallock (1969), who tested the depolarization characteristics of silica beach sand (0.1–0.5 mm particles), Haleakala volcanic ash (37–88 micron particles), and $MgCO_3$ (micron-size particles) for both coherent (He-Ne laser) and incoherent (tungsten iodine lamp) sources. They used a fixed viewing angle of 60° and varied the phase angle, wavelength, and polarization of the incident radiation. The depolarization of the scattered light varied with all these factors, but the the sand generally caused greater depolarization of the incoherent radiation than did the ash. Fig. 9 shows the polarization as a function of phase angle for those materials using the incoherent source. The authors attribute the lesser depolarization by the darker ash to its lower refractive component contribution. Although the substance composed of smaller individual particles led to less depolarization as in Egan et al. (1968), this is less of a fair comparison since it involves different substances altogether. More important to note in both soil studies is the overall number of variables that were involved, which highlights the complexity of depolarization by rough surfaces.

Curran (1978), in performing laboratory studies of polarization and soil moisture content, reemphasizes that polarization is a function of incident angle and the surface microtopography, which is determined by the soil's aggregate distribution and moisture content. In observations of brown sandy loam and red clay loam, he finds greater reflected polarization for finer particle sizes, but only above 60% soil moisture. Fig. 10 shows this correlation for soil at 100% moisture content. This trend stands in contrast to the opposite trend of the Egan et al., (1968) study, where polarization decreased with decreasing particle size. Notably, the Curran (1978) study used aggregrates and high soil moisture, while the Egan et al., (1968) study used dry ash sieved to various particle sizes.

The depolarization of electromagnetic waves by rough surfaces has been much studied theoretically, particularly in the context of radio waves scattering from irregular terrain or the sea surface. Fung (1966) used a mathematical technique known as the Kirchoff method to show that depolarization occurs for backscattering from dielectric surfaces. Valenzuela (1967), building on such previous studies, found that the form of the expression for depolarized scattered power matched the form found in multiple scattering studies.

16
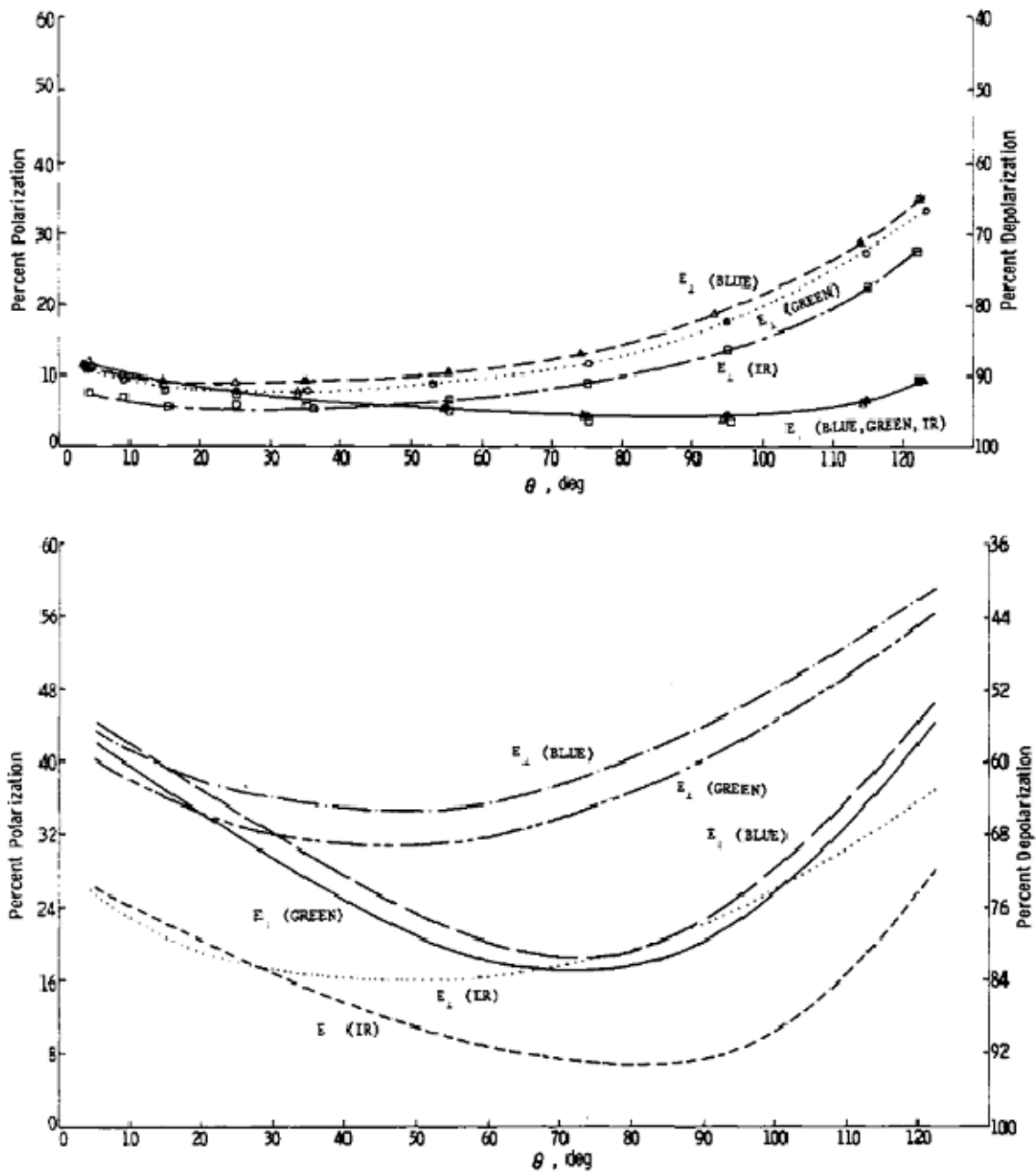
Figure 9.   Depolarization Characteristics of Sand (top) and Haleakala Ash (bottom) as a Function of Phase Angle for an Incoherent Source at Various Wavelengths (from Egan et al., 1969).

17
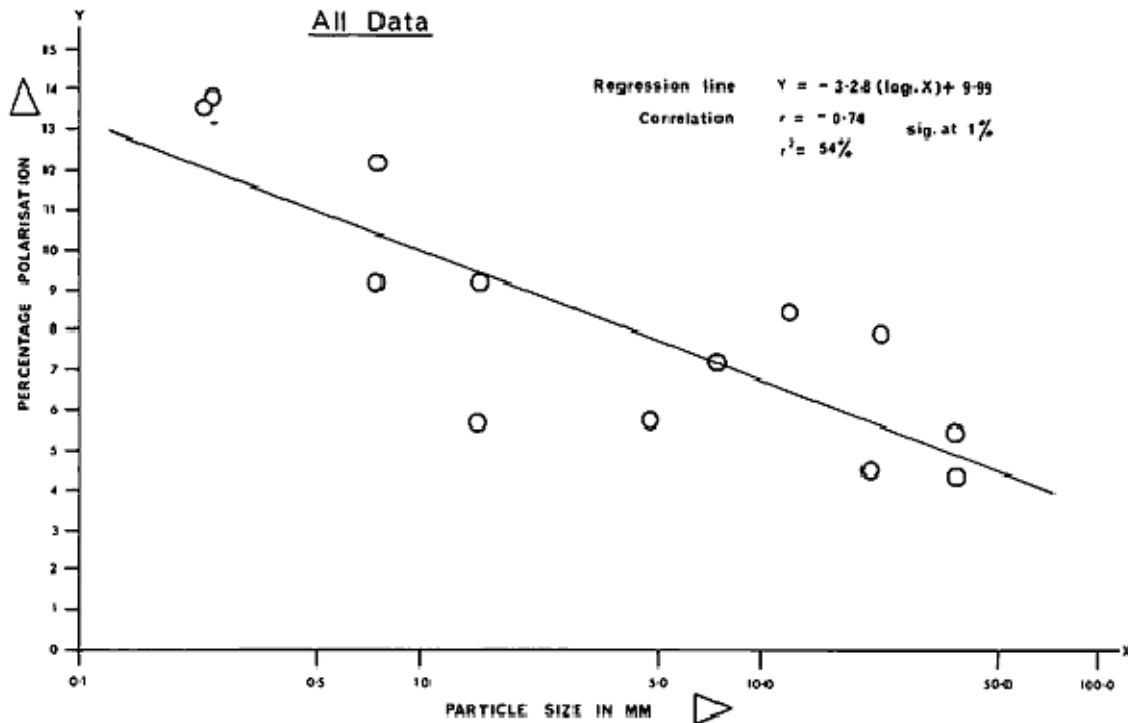
Figure 10.   Polarization of Two Loam Types (from Curran, 1978).

He concluded that multiple scattering is the cause of depolarization from slightly rough surfaces.

One manifestation of multiple scattering altering polarization is the Umov effect. Although natural smooth objects like grass or smooth stones may have a polarized "gloss," their main feature remains the diffuse reflection of the surface underneath. In such cases, the maximum degree of polarization of the reflected light is inversely related to the albedo of the material; i.e., the darker the object, the stronger its polarization. This relationship – the Umov effect – may be explained by the greater attenuation of multiply scattered (and hence less polarized) light on darker surfaces (Können, 1985). An early observation of this effect was the finding of Secchi (1859) that polarization of light reflected from the Moon was largest for darker regions. The findings of Egan and Hallock (1969) discussed above agree with the Umov effect as well.

18

III. METHODOLOGY

A. HARDWARE DESCRIPTION

Tyo et al. (2006) discuss the relative merits of several different types of polarimetric imaging systems. In a three-dimensional polarimeter, the Stokes parameters I, Q, and U are measured across a scene to find information about linear polarization. Such an imager is simpler and cheaper than one which measures V, since circular polarization is relatively complex to measure. The principal problem in three-dimensional polarimeters is acquiring images in the several different polarization states necessary to construct the Stokes parameters. The imaging must done simultaneously or as quickly as possible in order to minimize the effects of instrument or scene motion, which can lead to artifacts. The problem with the multiple images then becomes one of registration (proper alignment of the several images). Tyo et al. (2006) list a number of options for dealing with this issue, including co-boresighted imagers, division-of-amplitude imagers, division-of-aperture polarimeters, division-of-focal plane array imagers, and division-of-time imagers. These options vary in sophistication, and all have advantages and drawbacks, but the uncomplicated, robust, and relatively small option is the division-of-time imager. The concept is simple: the use of a filter that changes in time (e.g., mechanical rotation of polarization elements) in front of the camera to permit imaging of the different polarization states. Due to the time delay, this method is the least suitable for dynamic scenes, but such a device "can provide good results with a relatively small investment in hardware, design, and integration" (Tyo et al. 2006).

The polarimetric imager used in this research is a division-of-time polarimeter. Lefaudeux et al. (2007) of Bossa Nova Technologies, LLC note that while earlier time-division polarimeters that employed mechanical rotation were slow and sensitive to scene motion, electrically driven elements such as birefringent ceramics and liquid crystals have now allowed for fast time-division polarimeters. Their SALSA camera is such a device, employing fast programmable wave plates to detect linear polarization states of

$0°, -45°$, and $90°$. The wave plates alter the polarization state of the light passing through them and are able to switch between polarization states on a time scale of 100 μs.

This prototype camera is compact ($4'' \times 4'' \times 6''$) and robust. It employs a standard CCD (782×582 pixels) and standard F mount lenses (see Fig. 11). It uses 12-bit digitalization and can image at up to 35 frames per second in full resolution mode. The power supply is 15 V DC. Acquisition and image processing software run on a standard computer connected to the camera via IEEE-1394 FireWire and USB. The camera is integrated and calibrated with a 520 – 550 nm green filter (Lefaudeux et al., 2007).

The polarized filtering system can be broken down into two components: a 45-degree polarization rotator and a 90-degree polarization rotator. The 45-degree polarization rotator is itself composed of two elements: a quarter-wave plate and a programmable quarter-wave plate. To detect horizontally or vertically polarized light, the programmable plate is oriented such that horizontally or vertically polarized light will pass through both quarter-wave plates with its polarization unaltered. Light polarized at $45°$ or $-45°$ degrees will be converted to left-handed or right-handed circular polarization by the first plate, respectively, and the second plate is programmed such that these states will be converted to horizontal or vertical polarization, respectively.

Figure 11.   The SALSA Camera (from Lefaudeux et al., 2007).
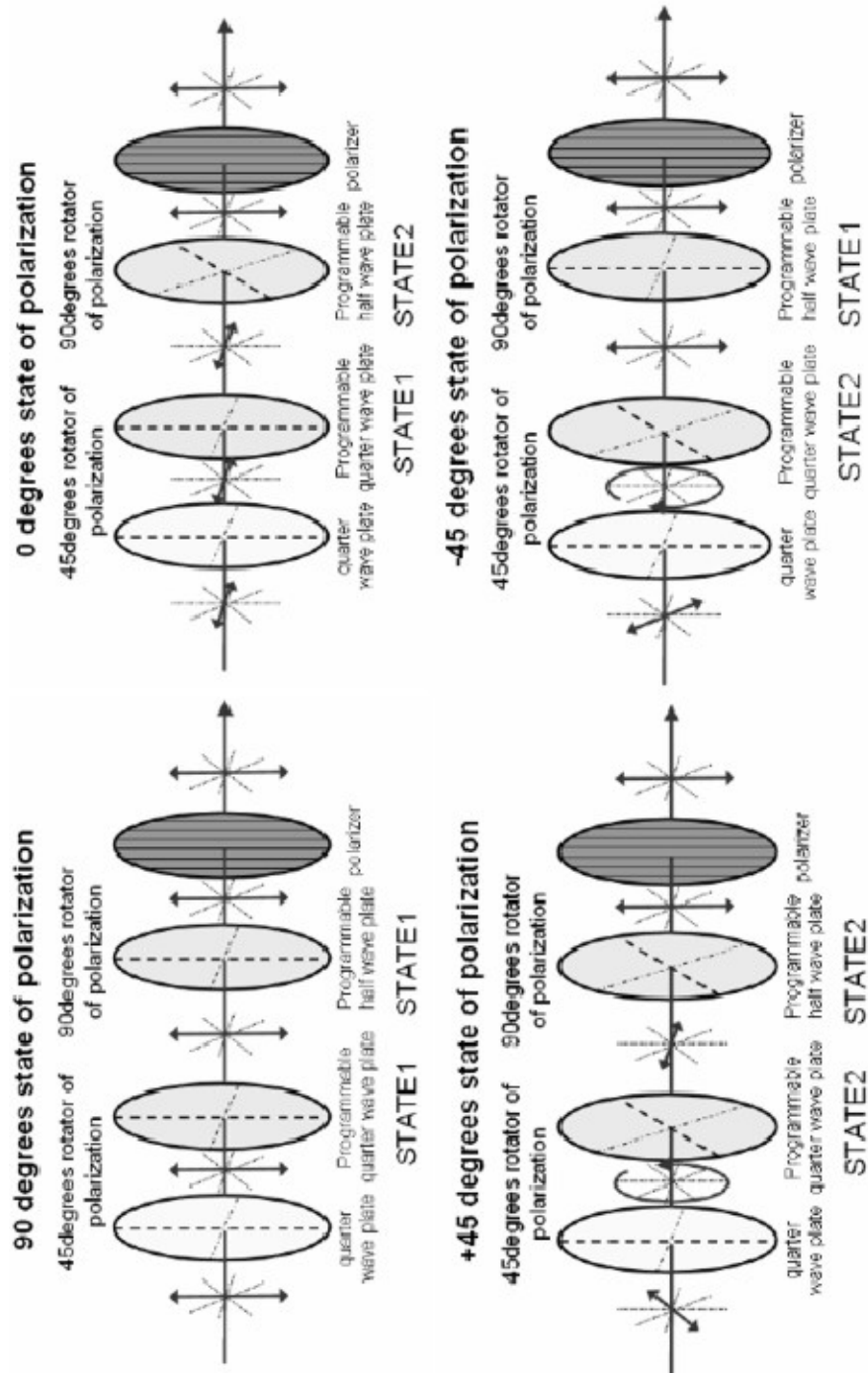
Figure 12.   SALSA Polarization Modulation (from Lefaudeux et al., 2007).

The 90-degree polarization rotator consists of a half-wave programmable plate and a vertical polarizer. To acquire the various states, the plate is set to the appropriate state to convert the desired incoming light to vertical polarization to allow it to pass through the polarizer to be detected by a standard CCD camera. Each of the four polarization states listed above has a unique sequence of wave plate settings that allows that polarization state to be detected (Lefaudeux et al., 2007). This whole concept is best understood in a diagram; see Fig. 12.

The software interface for the camera provides real-time visualization as well as options to record the data in various formats. The visualization options include the Stokes parameters, DOLP, and angle-of-polarization displays, along with several other possible variations and combinations. All can be mathematically reconstructed from the basic data – arrays containing the three Stokes parameters I, Q, and U measured across the CCD.

After calibration, the camera was shown to have excellent measurement capabilities; the standard deviation around a 100% DOLP measurement was 0.45%, which the manufacturer supposes can be further reduced by modifications. The standard deviation for measurements across other DOLP was 0.017% (Lefaudeux et al., 2007).

B.   GENERAL IMAGING PROCEDURES

The imaging performed in this thesis focused on "natural" (i.e., outdoor, relatively uncontrolled) scenery to partially simulate the situations where the camera would be used in practice. Some limitations were placed on the tests in order to facilitate the analysis of the results. Imaging was performed in clear conditions since the clear atmosphere and directionality of direct sunlight were supposed to favor polarization. The scenes were also chosen to control the amount of textural contrast and materials in the images.

Five sets of images are reported in this thesis: images of a "sandbox" still-life incorporating several soil and material textures, images of three paved areas with significant patching, images of a freshly re-dug and replaced patch of asphalt, images at several angles of a patch of dirt on a relatively smooth rooftop, and images of the Naval Postgraduate School peacock as a target of opportunity. In each case, exposure times

were chosen to obtain enough data while minimizing oversaturation in the field of view. Details of each data set are discussed in the next chapter.

C.   ANALYSIS TOOLS

The data were analyzed using version 4.5 of the Environment for Visualizing Images (ENVI™) software, an Interactive Data Language-based image processing package created by ITT Visual Information Solutions. Out of ENVI's large functional range, this study used basic image manipulation tools, texture filters, the region of interest separability tool, and the maximum likelihood classifier.

1.   Texture Filters

ENVI's texture filters are based upon the Haralick occurrence- and co-occurrence-based filters as set forth in Haralick, Shanmugam, and Dinstein (1973). In essence, occurrence measures count the number of appearances of each gray level within a user-defined processing window. The result is used to calculate data range, mean, variance, entropy, and/or skewness measures within the window, and the analysis is repeated as the window is moved across the entire image. Co-occurrence measures are based on Haralick's gray-tone spatial-dependence matrices, which relate gray level values to those in nearby cells. These matrices are used to calculate measures of the mean, variance, homogeneity, contrast, dissimilarity, entropy, second moment, and correlation of the gray tones within the processing window. As with the occurrence measures, these quantities are calculated as this window is moved across the image (see also Humphrey, 2003 and Puetz, 2006 for terrain classification and spectral applications).

It should be noted that here, "texture" refers to the visual texture in the image—the variability in gray tone across a region – rather than the physical texture of the objects being imaged. Although it is true that the two may well be related, it is important to realize that the texture filters operate on the visual texture in the array of gray-tone values it receives from the camera.

2. Region of Interest Separability

ENVI is able to calculate the spectral separability of user-defined regions of interest based upon statistical measures of the gray levels in those regions. Of the two separability measures reported by ENVI, this study reports the Jeffries-Matusita measure, which has values ranging from 0.0 to 2.0. Values higher than 1.9 indicate good separability, while values lower than 1.0 are undistinguishable (Richards, 1999).

3. Maximum Likelihood Classifier

According to Richards (1999), maximum likelihood (ML) classification is the most widely used and often the most effective means of supervised classification in remote sensing. The classification is based upon the statistics of chosen regions of interest. The algorithm assumes that the statistics for each class are normally distributed in all bands and uses a Bayesian decision rule to calculate the probability that each pixel in an image belongs to a given class. The pixel is then assigned to the most likely class (Richards, 1999).

IV.   OBSERVATIONS

A.   "SANDBOX" IMAGES

The primary disturbed-earth test was a semi-controlled experiment on the roof of Spanagel Hall. The author filled a box with beach sand and placed a tray filled with Sheridan coarse sandy loam from the local area on top of the sand. Half the dirt tray was covered with loose soil and half of it was packed down. A cardboard rectangle and several polarizing filters were added to the scene for reference purposes.

This sandbox was imaged in clear conditions during late afternoon from an angle looking directly toward the descending Sun (hereafter referred to as the head-on view) and from an angle about $20°$ off of that line (hereafter referred to as the offset view). The Sun was roughly $60°$ above the horizon, and the camera was pointed approximately $20°$ below the horizontal at a range of 16 feet from the box using a standard Nikon lens at f/5.8. Practicalities prevented imaging from a full range of angles around the box, but it was anticipated that the best polarimetric imaging results would be apparent looking directly into the Sun. Consequently, the head-on and offset views were considered sufficient as an initial indicator of the camera's disturbed-earth detection capability.

The images at these two angles are shown in Fig. 13. They show the Stokes parameters and DOLP. The polarizing filters are clearly visible as very dark or bright squares, depending on the filter orientation and the parameter displayed. Ordered from left to right, and measuring the filter angle counterclockwise from the horizontal, the polarizers are oriented at $0°$, $90°$, $45°$, and $135°$. The cardboard is visible to the right in the sand, and the dirt tray with its disturbed and undisturbed portions is located to its left.

All eight images were generated in ENVI software using a 2% linear stretch. It should be noted that because the Q and U images are polarization difference images, they include both positive and negative values. This causes a visualization problem, since the center of the stretch window determines the gray tone level corresponding to a value of zero in either of those parameters. The 2% stretch applied here and throughout much of

this thesis was chosen for display purposes, but for analysis, when looking at Q and U in ENVI, the author suggests using a symmetrical stretch and a color mapping such as "Blue-Red," which will apply differing hues to positive, negative, and near-zero polarization difference values.
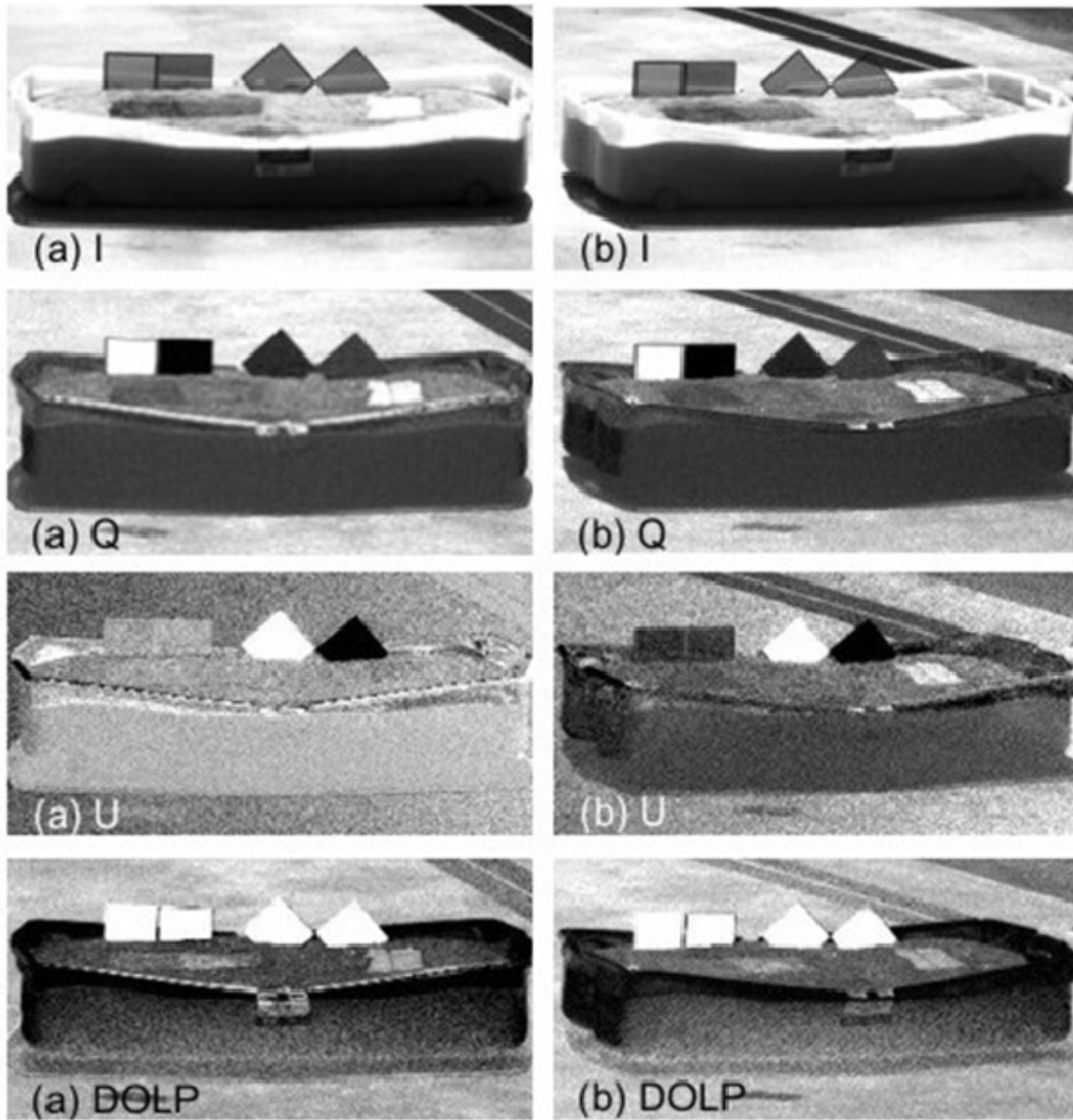

Figure 13.   Head-On (a) and Offset (b) Sandbox Images (7 May 2009, ~1530).

Such a color mapping is displayed in Figs. 14 and 15 for both Q and U using the colors blue and yellow. Grayish mixed hues correspond to mild or near-zero polarization difference values. Note the difference in scaling between Q and U.
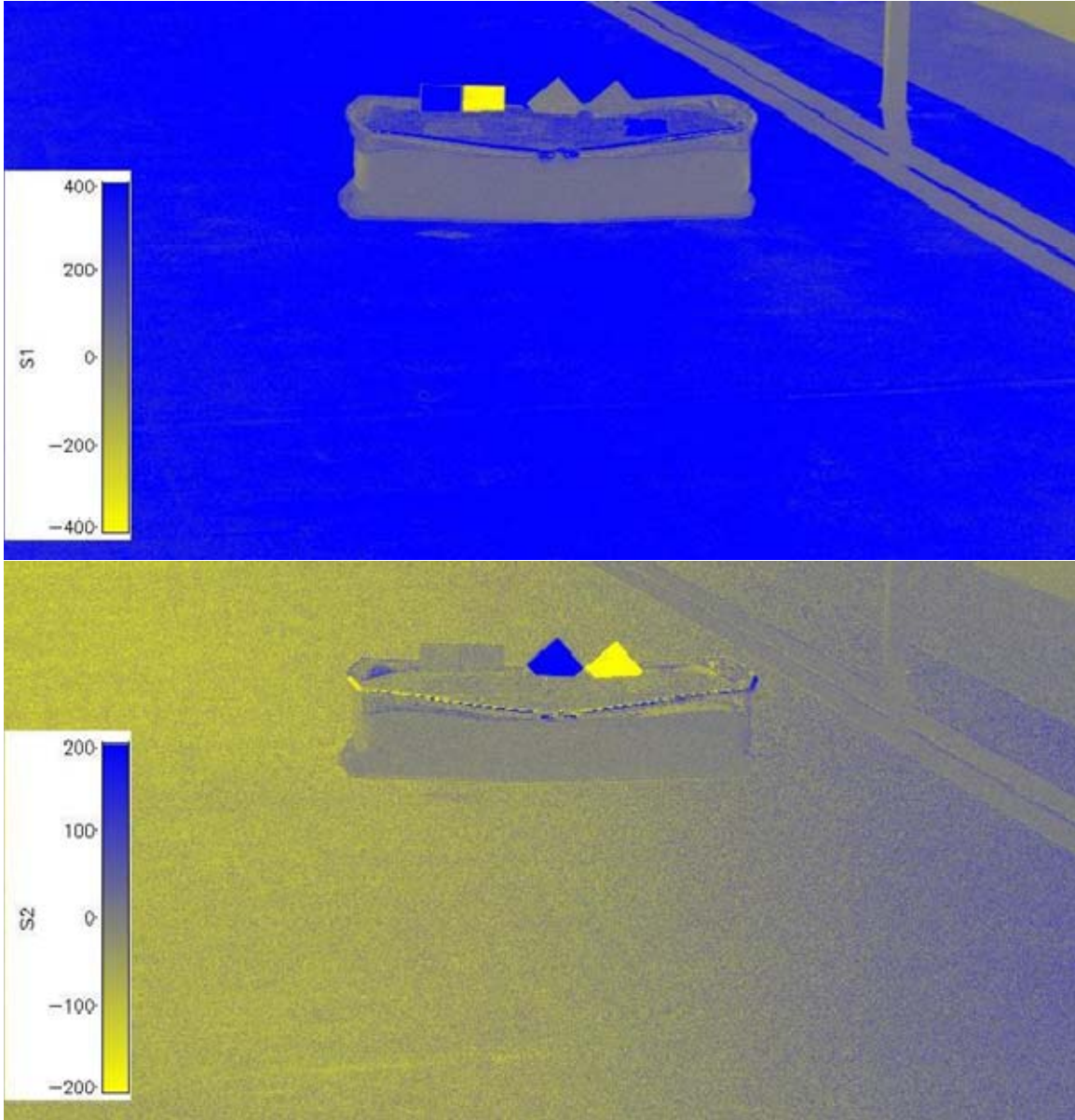

Figure 14.   Head-On View, Blue-Yellow Scaling

In these views, the shadowed areas are clearly not strongly polarized. In the 2% stretch, however, shadowed areas can appear "noisy" in polarization: where there is not much light, one near-zero value is being subtracted from another, resulting in apparently

random values for the polarization. It should also be noted that there can be slight contrasts between filters even in images where differences should not occur (e.g., between the 45° and 135° filters in the $0° - 90°$ images). Repeated experimentation showed that this is simply due to the high sensitivity of the images to filter orientation.
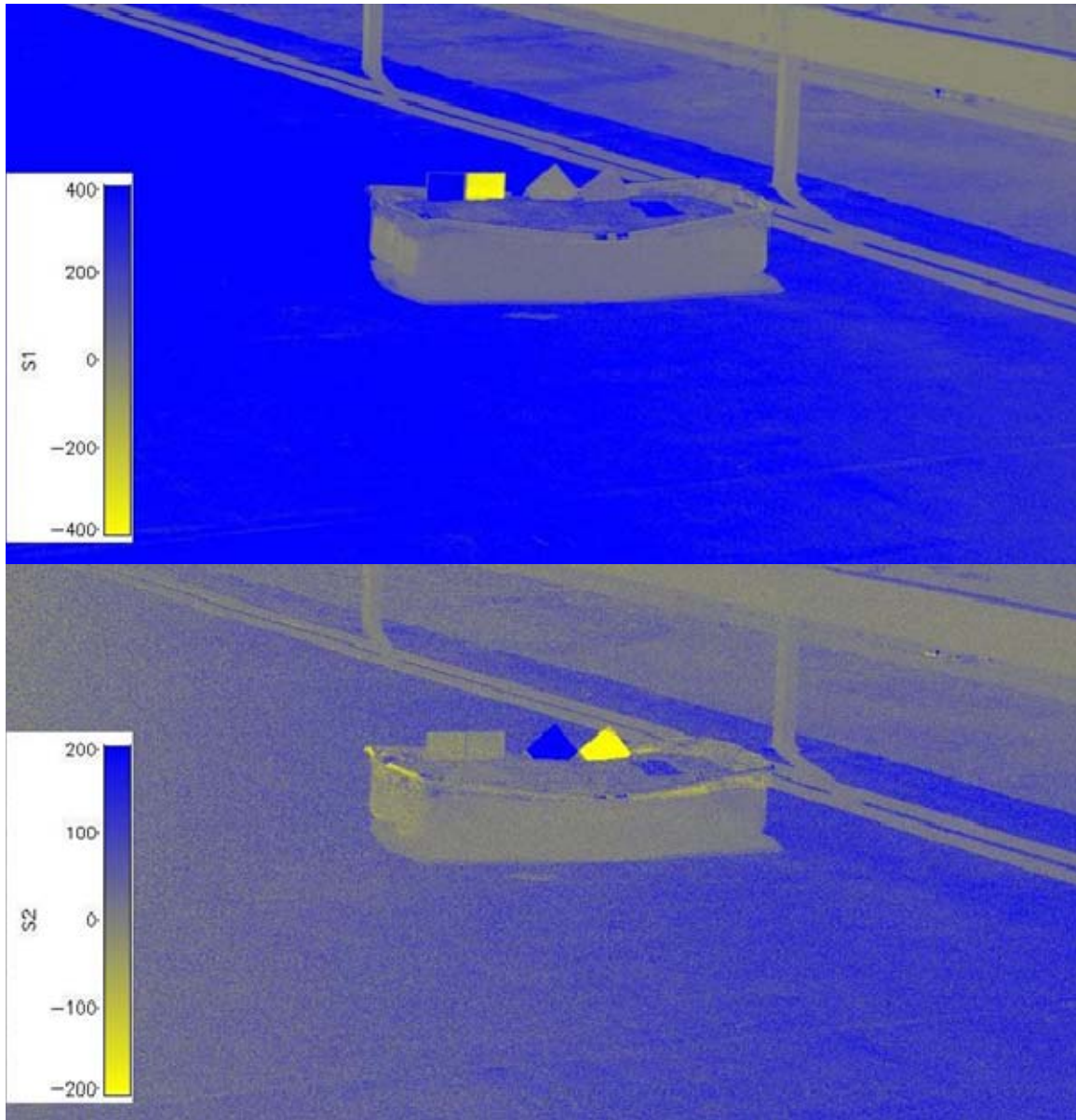

Figure 15.   Offset View, Blue-Yellow Scaling

In these sandbox images, the primary difference of interest is the visible difference in DOLP between the loose and the packed patches of soil, since this is the

28

best simulation of disturbed against undisturbed earth. This difference is apparent in several bands, including intensity and DOLP, though the difference is not as sharp as that between cardboard and sand. The disturbed/undisturbed contrast is more significant in the $0° - 90°$ images.
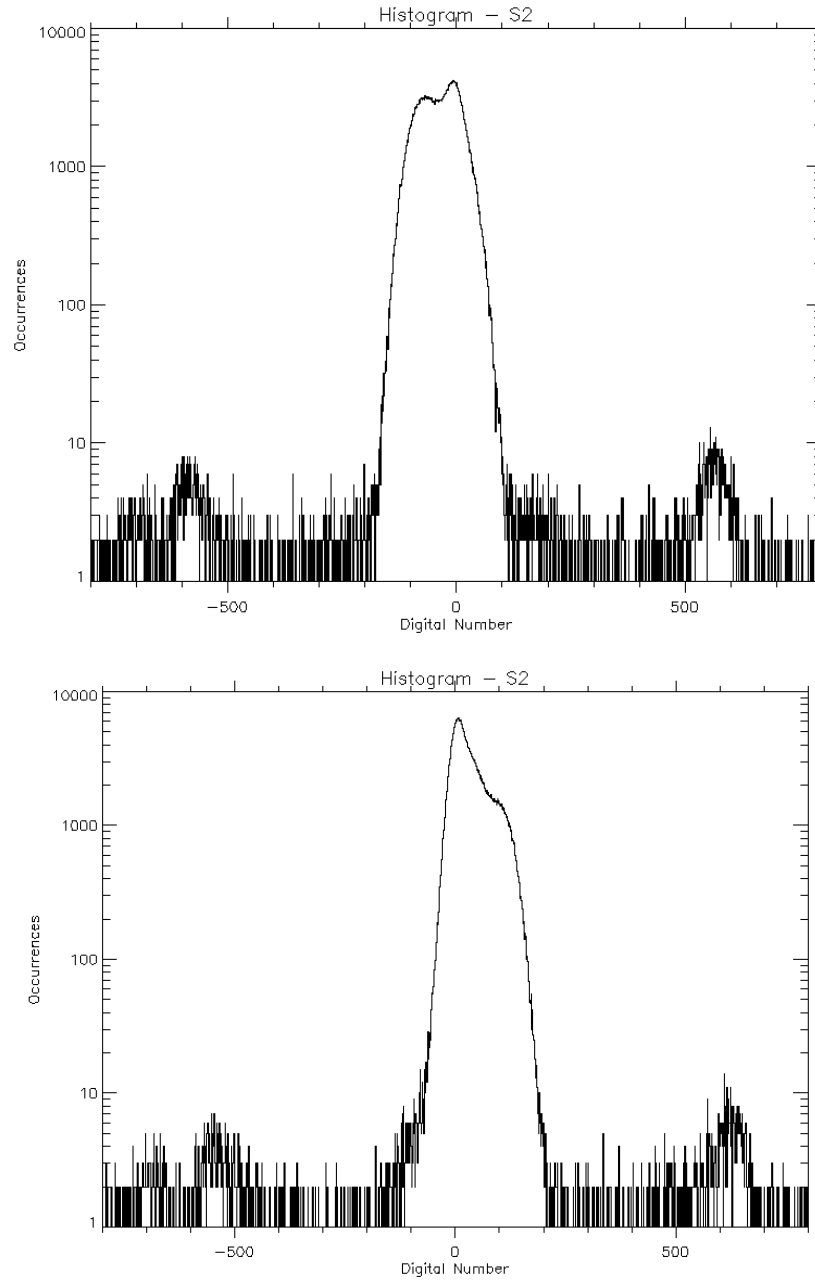

Figure 16.   Histograms of U for Sandbox Head-on (top) and Offset (bottom).

It is also instructive to plot histograms of the polarization difference images. Histograms of U in the head-on and offset views are shown in Fig. 16. The outlying features come from the light from the two filters at their perpendicular orientations, while the large central features result from reflection by the other elements in the image. The histogram is nearly symmetric in the head-on view. This is to be expected; since the light source is head-on and the surfaces in the image are primarily horizontal and vertical, neither 45° nor 135° polarization ought to be preferred. In the offset image, however, the symmetry is broken by the differing positions of the outlying features and the skew of the central feature. This asymmetry is a consequence of the asymmetry in lighting; because the light source is off-axis, it is possible for one polarization to be preferred over another.

The sandbox was also imaged in a close-up using a standard Nikon zoom lens. The result, displayed in Fig. 17, illustrates a difficulty with disturbed-earth detection. The DOLP varies sharply from dirt grain to dirt grain, which the camera may be able to resolve (depending primarily on its distance from the target dirt patch). For disturbed-earth observations, however, the aggregrate polarization characteristics of a given patch are of greater interest. This fact necessitated the use of statistical tools to look at the results, as discussed in the next chapter.
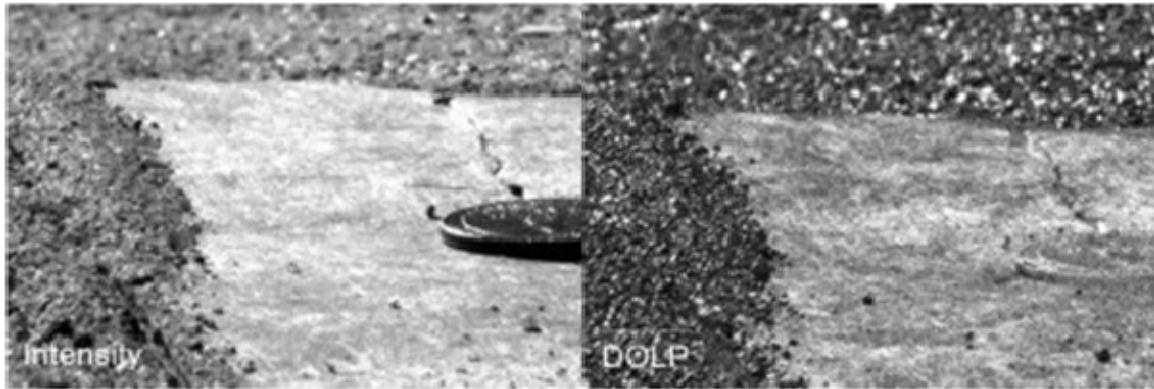

Figure 17.   Sandbox Close-up with Quarter (7 November 2008, ~1530).

B.   PARKING LOT IMAGES

To test the camera's ability to distinguish the polarimetric characteristics of asphalt of different ages, the author took images of three sites with significant asphalt patching. The first site was parking lot S at the Naval Postgraduate School. Intensity and DOLP images at various angles are shown in Fig. 18. To varying degrees, the difference between patches and the neighboring asphalt is visibly evident in both intensity and DOLP in most of the images. The triangles indicate the general direction toward the Sun.

The polarimetric camera is truly useful in augmenting visual search only if it is able to spot differences where they are not already obvious in intensity. The second and third asphalt sites were chosen because they had patching that was similar in appearance to the original paving. One was a street in the La Mesa residential area in Monterey, CA, and the other was a parking lot area between the chapel and gym at the Naval Postgraduate School. Some intensity and DOLP images of these lots are shown in the following chapter.
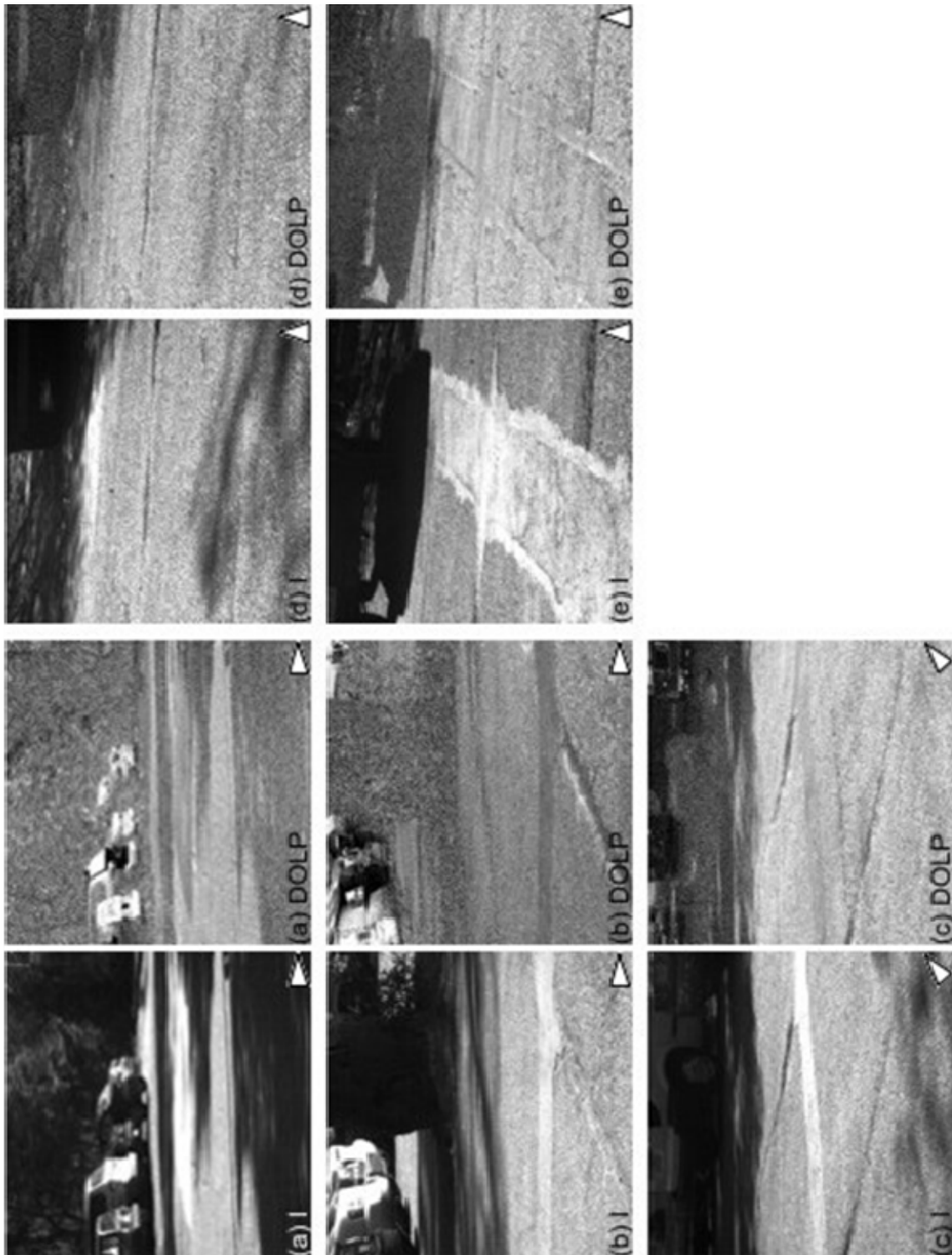
Figure 18.   Naval Postgraduate School S Lot (21 November 2008, 1320 – 1330).
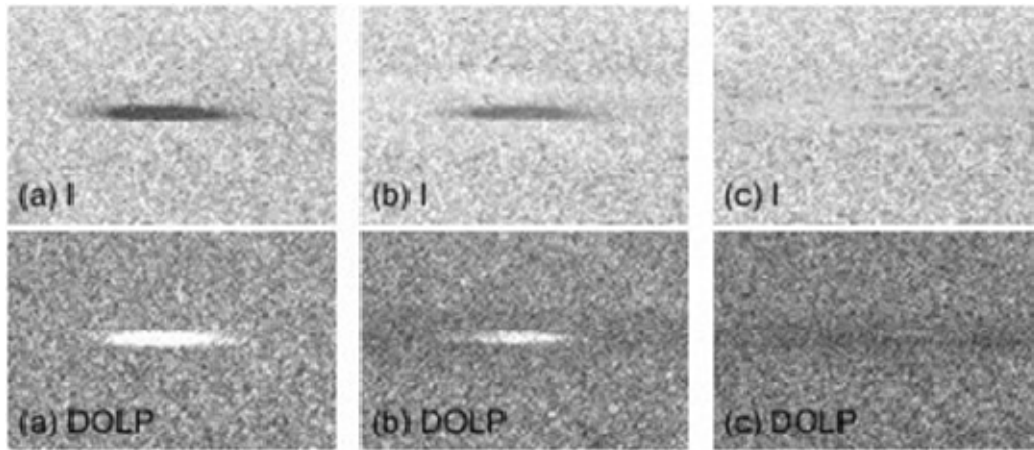
Figure 19.   Disturbed Asphalt with Varying Dirt Coverage (5 May 2009, 1445–1500).

C.   DUG & REPLACED ASPHALT

The author softened, dug up, and replaced a small patch of asphalt on a former Fort Ord road (Marina, CA) to see whether the signature of old but freshly disturbed asphalt was similar to that of an asphalt patch. The patch was imaged 24 hours after the disturbance, both with and without partial dirt coverage, and it was imaged eight days after the disturbance, having been dirtied and driven over several times. In both cases, the general direction toward the Sun is toward the upper right in the images. Initially, the patch looked quite fresh (since the newly exposed sub-surface asphalt was unweathered), so it was obvious in both intensity and DOLP. Without any dirt cover, the signature of the turned-up asphalt was quite strong, showing 100% DOLP, but it became less prominent as dirt cover increased (see Fig. 19, with dirt coverage increasing left to right).

Eight days later, the patch was just as distinct in both intensity and DOLP (see Fig. 20), showing that the polarization signature remains quite strong for at least that relatively brief time period.
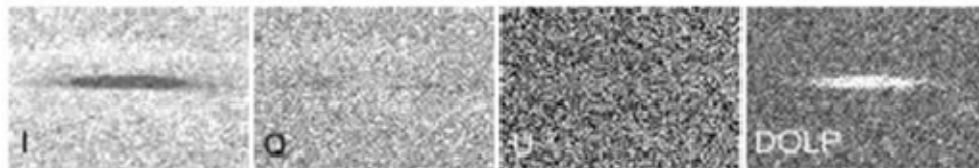

Figure 20.   Disturbed Asphalt after Eight Days (13 May 2009, ~1525).

33

It should also be noted, however, that the patch is practically invisible in the more "pure" polarization parameters Q and U. This was also true of the images taken 24 hours after the fact. This fact is addressed further in the next chapter.

D.   ROOF IMAGES

The author also imaged a patch of dirt on the roof of Spanagel Hall from several angles. This test was a good multi-angle case where the difference in texture (and intensity) was very obvious. Fig. 21 shows intensity and DOLP images from four angles with respect to the direction toward the Sun. Again, the triangles point in the general direction of the Sun. Image (c), with the Sun behind, required a steeper viewing angle due to space constraints on the roof. The dirt appears the same in all four intensity images—darker than the roof—but it appears darker in DOLP in the head-on image (a) and lighter than the roof in the sidelit images (b) and (d). The dirt patch is not quite visibly apparent in DOLP in image (c).
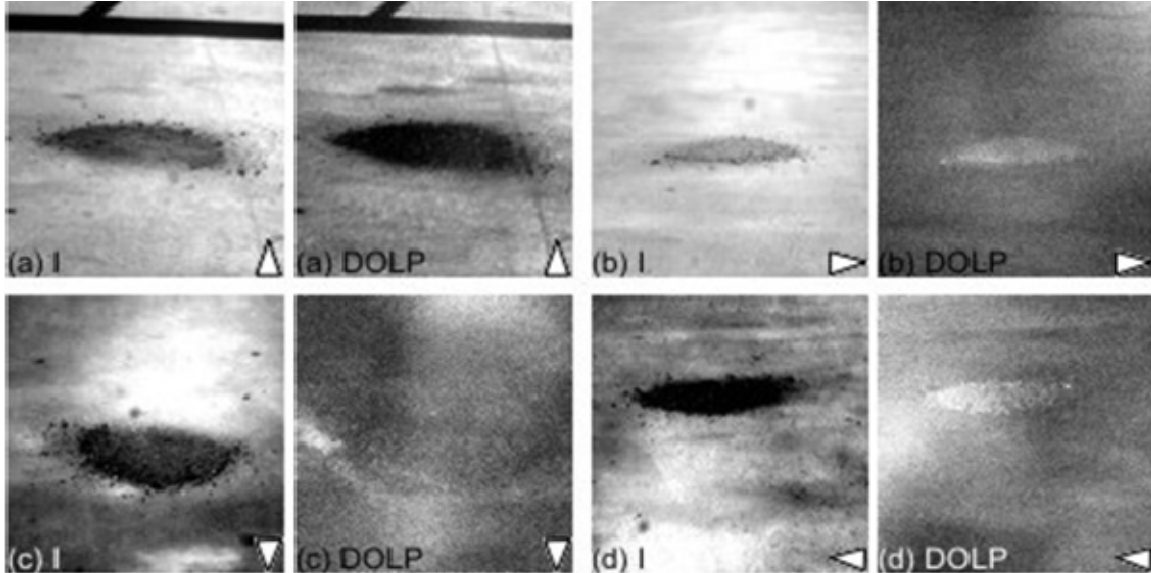

Figure 21.   Dirt Patch on Spanagel Hall Roof (22 Oct. 2008, 1120–1130).

E. PEACOCK IMAGES

The Naval Postgraduate School peacock presented a target of opportunity during the chapel/gym lot imaging and was captured using the polarimetric camera. Some results in intensity and DOLP are presented in Fig. 22 along with a color photo of the same bird taken with a standard store-bought digital camera. (Note that in the SALSA images, his feathers appear to be folded, not spread.) In SALSA image (a), the peacock appears quite distinct in DOLP, though he is invisible in the shade in intensity. In (b), he is visible in DOLP only because of his silhouette – he seems to be facing either toward or away from the camera, so his long feathers are not reflecting and polarizing the light as they are in image (a). These images show that at least for some angles, peacock feathers have a strong polarizing effect.
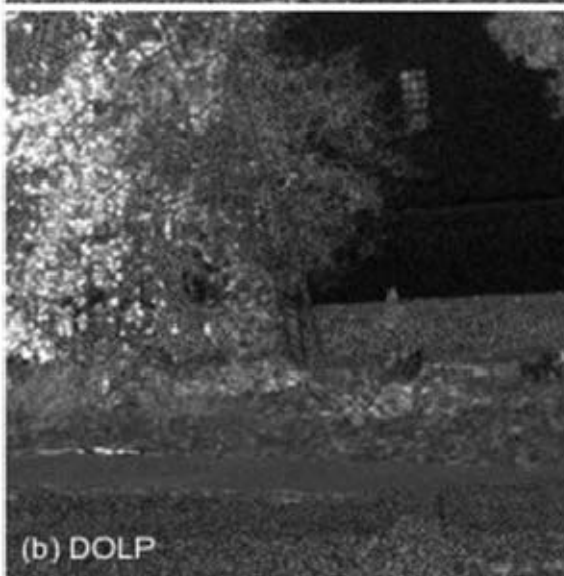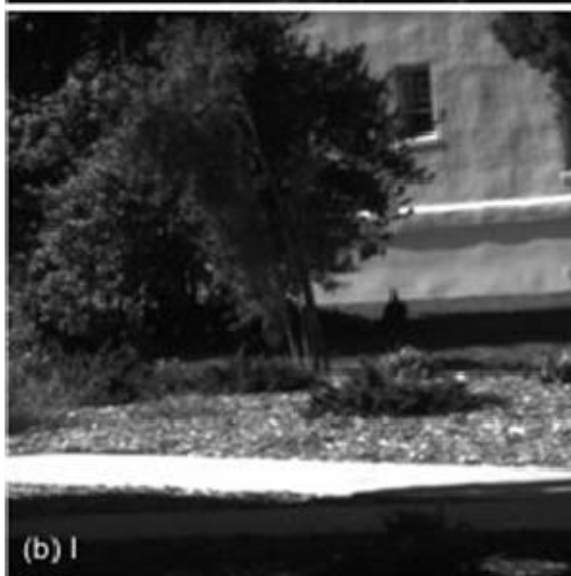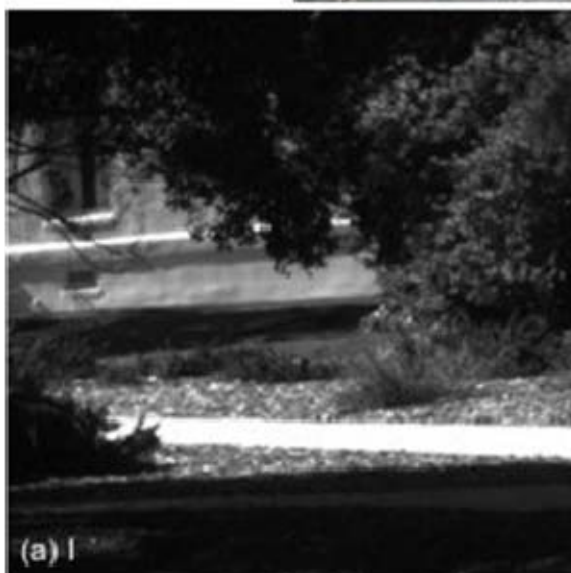
Figure 22.   Peacock in Color (8 April 2009) and in Shadow (23 March 2009).

V. ANALYSIS

A. TEXTURE FILTERS

Without image processing, the difference between disturbed and undisturbed earth and old and new asphalt is not as readily visibly apparent as might be hoped. In an attempt to enhance the polarization signature, the images were run through a number of occurrence- and co-occurrence-based filters of several window sizes, and, in the case of the co-occurrence filters, two different shift values. ROI separability was then calculated for some of the results.

1. Occurrence Measures

Fig. 23 shows the regions of interest (ROIs) in the sandbox image. The appendix shows tables of DOLP images run through occurrence filters for the sandbox head-on, the sandbox offset, and one view of the Spanagel Hall S Lot. In the sandbox images, the visible distinction between the disturbed and undisturbed soil is not very significant under any filter type or window size, although there is a slight difference visible in the mean for the offset image for the smaller processing windows. In the parking lot images, no significant enhancement is provided by occurrence processing. It may be supposed that in the case of the mean, the images are taken from such a distance that the texture is not smoothed significantly by the mean filter.
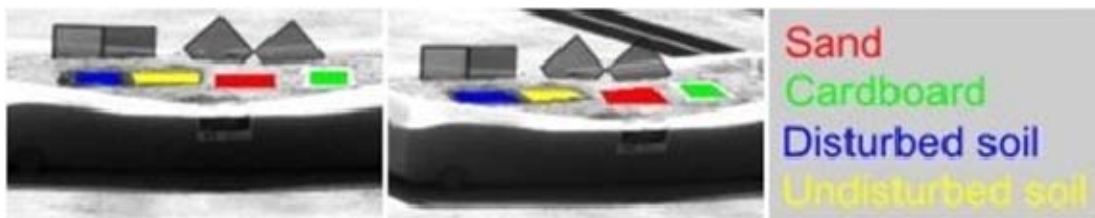
Figure 23. Sandbox ROIs from Two Angles (7 May 2009, 1520–1530).

## 2.	Co-occurrence Measures & ROI Separability

The appendix shows tables of sandbox (head-on) and S Lot DOLP images run through co-occurrence filters. Processing window shifts of one unit (in both x and y) and three units (in both x and y) were tested, since the textural measures depend on the scale of the visual texture. (The shift direction was chosen arbitrarily, since the visual texture of the soil or asphalt does not depend on direction.)

In general, many of the co-occurrence measures did not help to distinguish between surfaces, but there were several exceptions: undisturbed soil differed from sand and disturbed soil under entropy, second moment, and correlation filters under some processing window sizes. The sand and disturbed soil themselves were not visibly distinct. These three measures were chosen as the basis for computation of ROI separability of the undisturbed soil from the other surfaces using the Jeffries-Matusita measure previously discussed. The results are plotted in Figs. 24 and 25. The legends list the combinations of processing window size and shift value attempted.
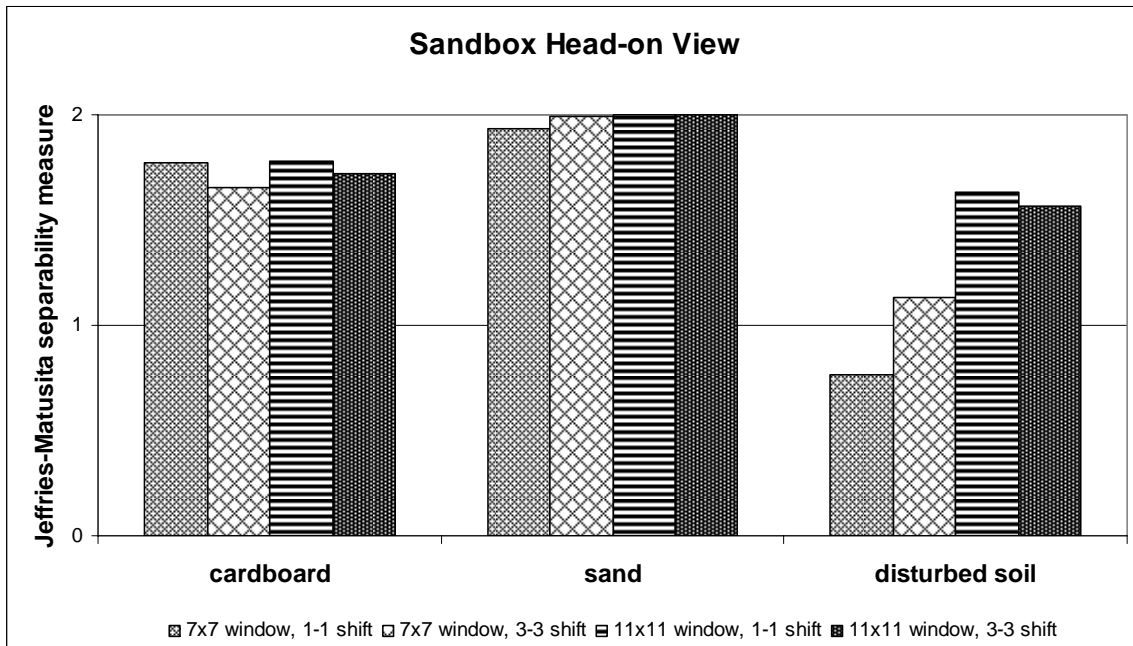

Figure 24.	ROI Separability of Sandbox Undisturbed Soil.
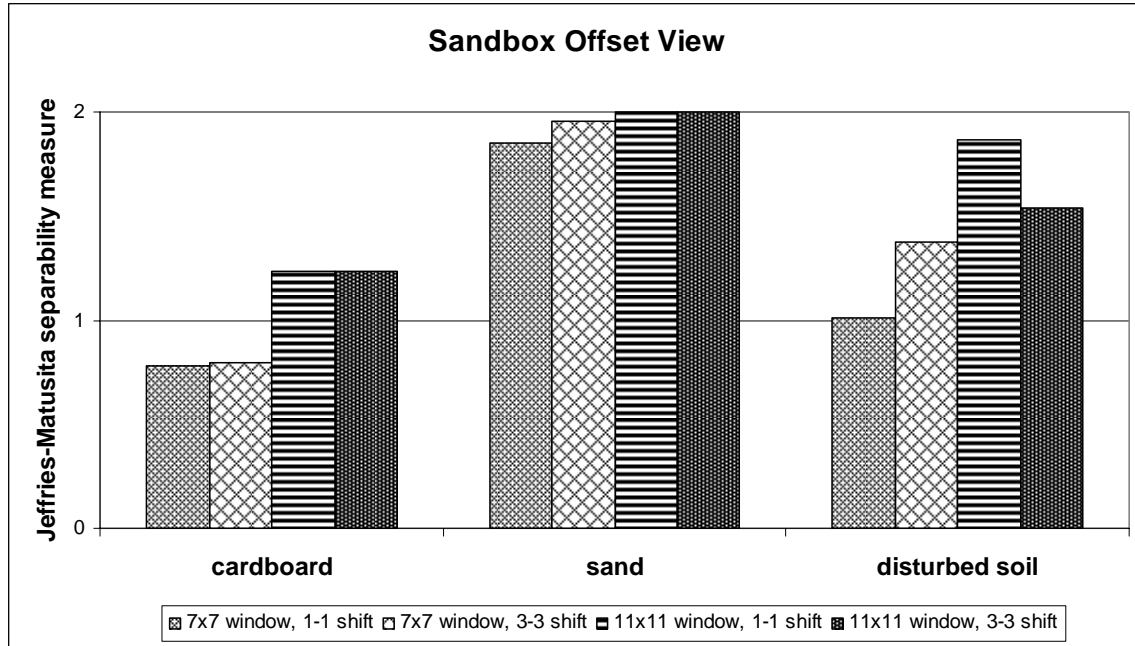
Figure 25.   ROI Separability of Sandbox Undisturbed Soil.

In the head-on view, the undisturbed soil is fairly separable from cardboard and fairly separable from sand for all window/shift combinations. It is not very separable from disturbed soil, though separability shows a marked improvement with larger processing window size. In the offset view, the undisturbed soil shows good separability from sand, but poor separability from cardboard. For disturbed soil, the 11×11 processing window and 1-1 shift achieved fair separability, with small improvements visible in the other window/shift combinations as well.

From these results, it appears that viewing angle, processing window size, and shift value all matter.   In particular, for disturbed/undisturbed soil, better separability occurs for a processing window size nearer to the scale of the area of concern. Also, separability between these two regions is only significant in the offset view for a particular window/shift combination.

In the S Lot images, entropy and second moment again "pull out" the differing textural features (see the appendix). Correlation still helps as well, but not as much as homogeneity filtering, which has gone from being a mediocre help in the case of the

39

sandbox to a good aid in the case of asphalt. Particularly in homogeneity and second moment, a second patch of asphalt further in the background becomes apparent that is not visible in DOLP. As with the sandbox, processing window size matters: the patches are more easily distinguishable as the window size approaches the scale of the disturbance.

B.   MAXIMUM LIKELIHOOD ANALYSIS

1.   S Lot

A maximum likelihood (ML) analysis of the S Lot images was conducted using the ML classifier included in the ENVI package. The analysis was performed once based on all four bands and once based only on polarimetric bands (Q, U, and DOLP) using ENVI rule images. Fig. 26 shows a subset of an image with its user-selected ROIs; red was chosen for the older asphalt, while cyan was chosen for the patching.

The results of the ML classification are shown in Figs. 27 and 28 based on sets of bands including intensity and not including intensity, respectively. Color-coding indicates whether areas are classified as one or the other ROI-based class, with pure color representing a likelihood value of zero (100%) that that point belongs to that class. Black indicates points not classifiable either way. Both with and without including intensity, the result is strikingly clear, and the plots of ROI DOLP values show excellent separation. Purely polarization-based ML classification is slightly less successful than that including intensity, but the result is still so sharp that it indicates that the ML classifier may be able to find good separation even without large intensity differences.
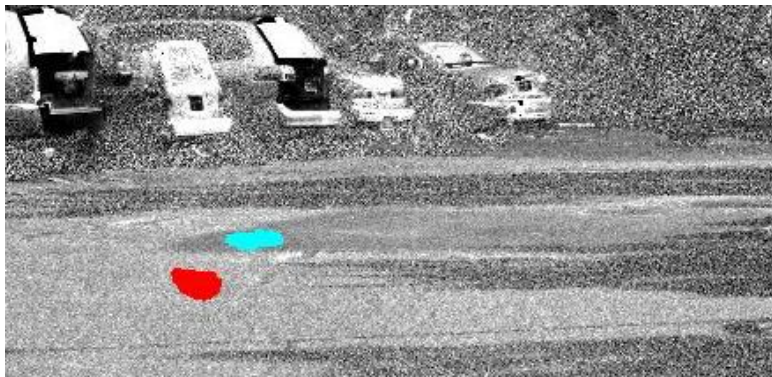

Figure 26.   S Lot User-Defined ROIs.
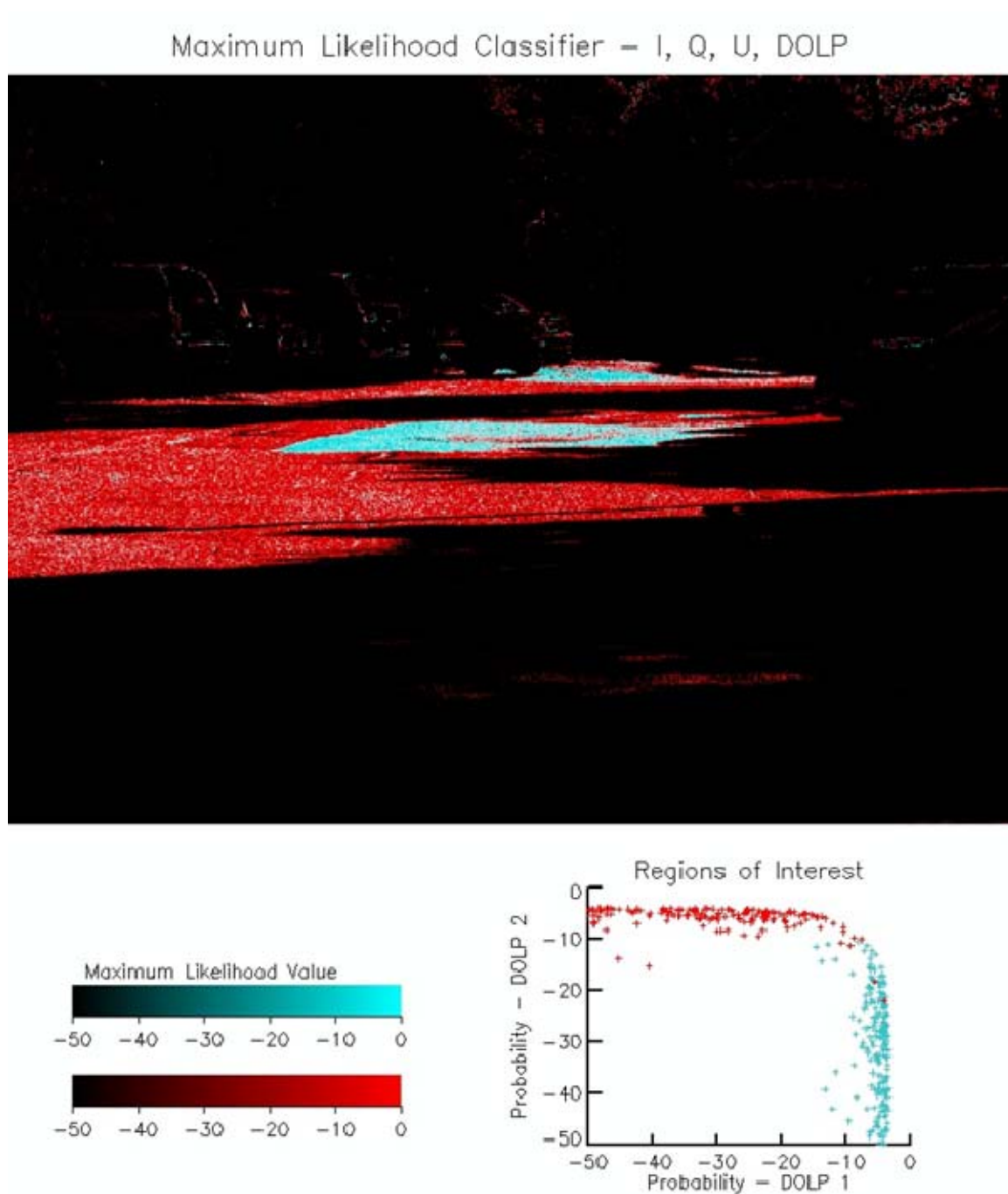
Figure 27.   S Lot Polarimetric and Intensity-based ML Classification
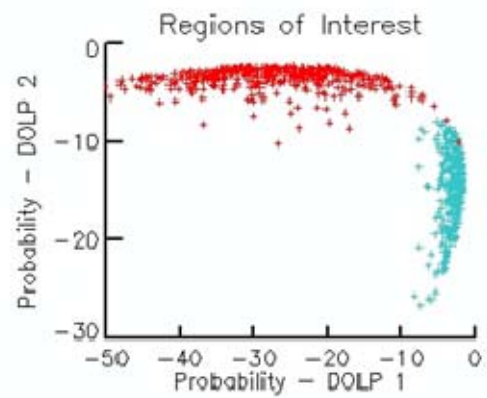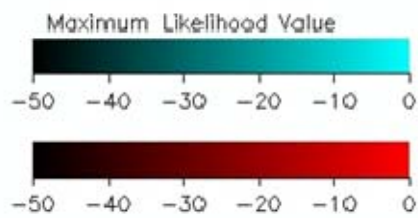
Figure 28.　　S Lot Polarimetric ML Classification
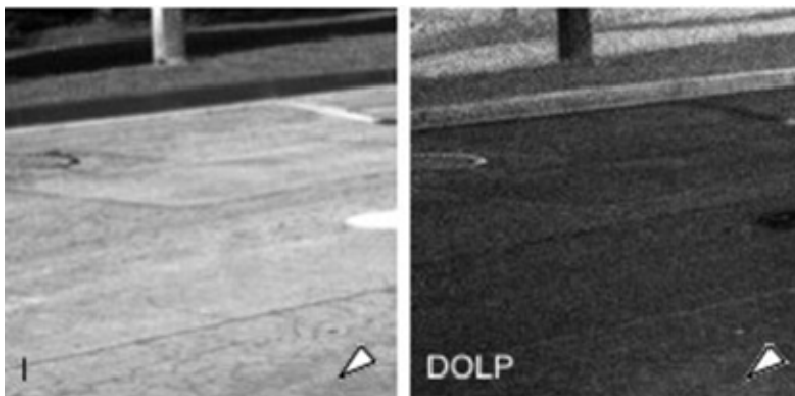
Figure 29.   Patch in La Mesa Street (27 February 2009, ~1330).

2.   La Mesa Lot

The ML analysis conducted in the La Mesa area showed no significant difference between original paving and patching. The ML outputs are omitted here for brevity; however, a sample image in intensity and DOLP is included in Fig. 29 above. The lack of contrast in the images and the ML analysis is likely a consequence of both original paving and patch being quite aged; both are apparently old enough that any age difference between them does not show well. This was true regardless of viewing aspect.

3.   Chapel/Gym Lot

As in the S Lot, the chapel/gym lot ML results were positive. One patch was particularly interesting since it was less obvious in intensity. Intensity and DOLP images, with the corresponding regions of interest, are shown in Fig. 30. The edge of the patch is a bit shadowed in intensity, but the bulk of the patch is not distinguishable from the adjacent pavement. In DOLP, however, the entire extent of the patch is obvious. This indicates that for at least some cases, polarimetry can distinguish asphalt age even when it is not otherwise apparent.

As can be seen in Figs. 31 and 32, the ML classification results successfully extracted the asphalt strip running just below the painted traffic arrow. The intensity data (see Fig. 31) provides some benefit over the purely polarimetric image (see Fig. 32),

primarily in eliminating heavily shadowed areas in the image from classification. On the other hand, intensity does not seem to add much benefit in extracting the asphalt patch of interest. Based on this fact and the comparison of intensity, Q, U, and DOLP in Fig. 30, most of the information about the asphalt strip comes from polarization.

4. Dug & Replaced Asphalt

Although a ML analysis was not conducted on the dug/replaced asphalt, it is worth comparing it to the chapel/gym lot results discussed above. It is apparent from Figs. 30, 31, and 32 that it is polarization rather than intensity that distinguishes the strip of patching. The opposite, however, seems to be true of the dug/replaced asphalt, where there is no signature in Q and U, but in DOLP, the signature is obvious (see Fig. 20). This suggests that in the absence of a strong polarization signature, the DOLP image simply inverts intensity. Taking that view, DOLP is not carrying additional information.

Alternatively, one might say from Q and U that in spite of its darker color, the dug/replaced patch was as polarizing as the surrounding weathered asphalt, leading to the strong signature in DOLP. In this interpretation, DOLP is carrying additional information (albeit information that is already obvious in intensity). As the dug/replaced patch ages, it may be that it will retain a stronger polarization signature even as weathering reduces its visibility in intensity. This is an important question, since the usefulness of polarimetric imaging lies in its ability to distinguish surface differences where they are not otherwise obvious.


Figure 30.   Chapel/Gym Lot with Regions of Interest (23 March 2009).
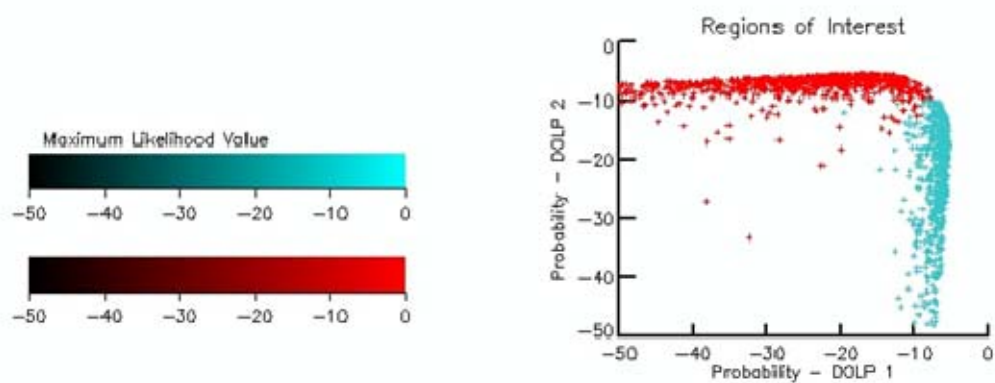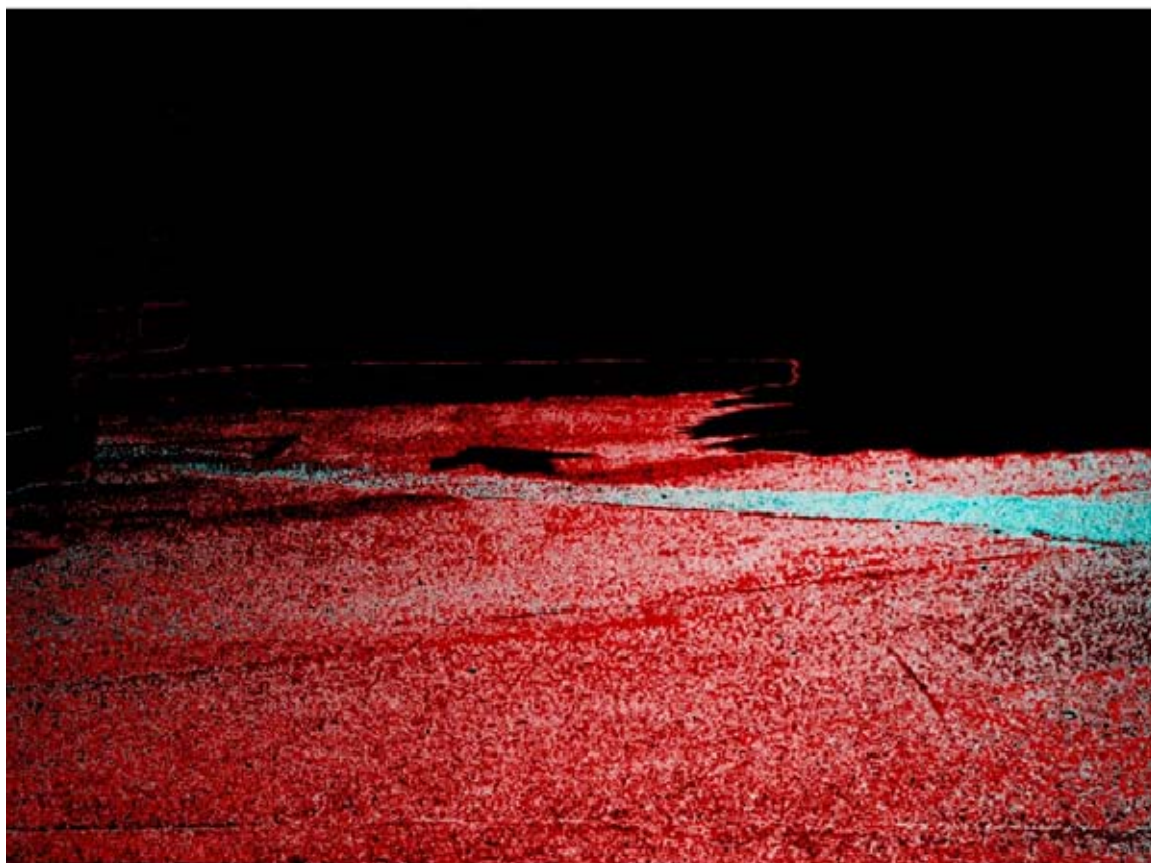
Figure 31.   Chapel/Gym Lot ML Classification Including Intensity.
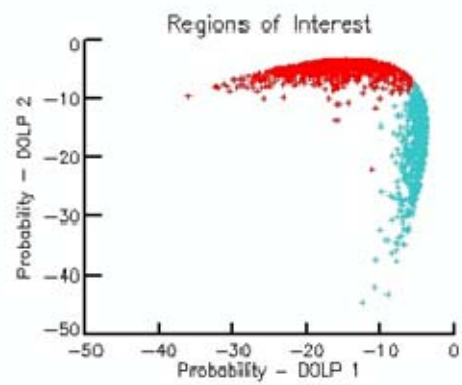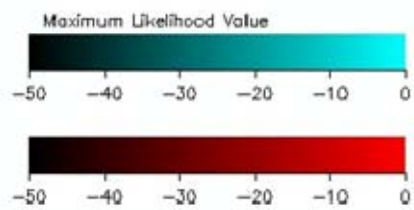
Figure 32.   Chapel/Gym Lot Polarimetric ML Classification.
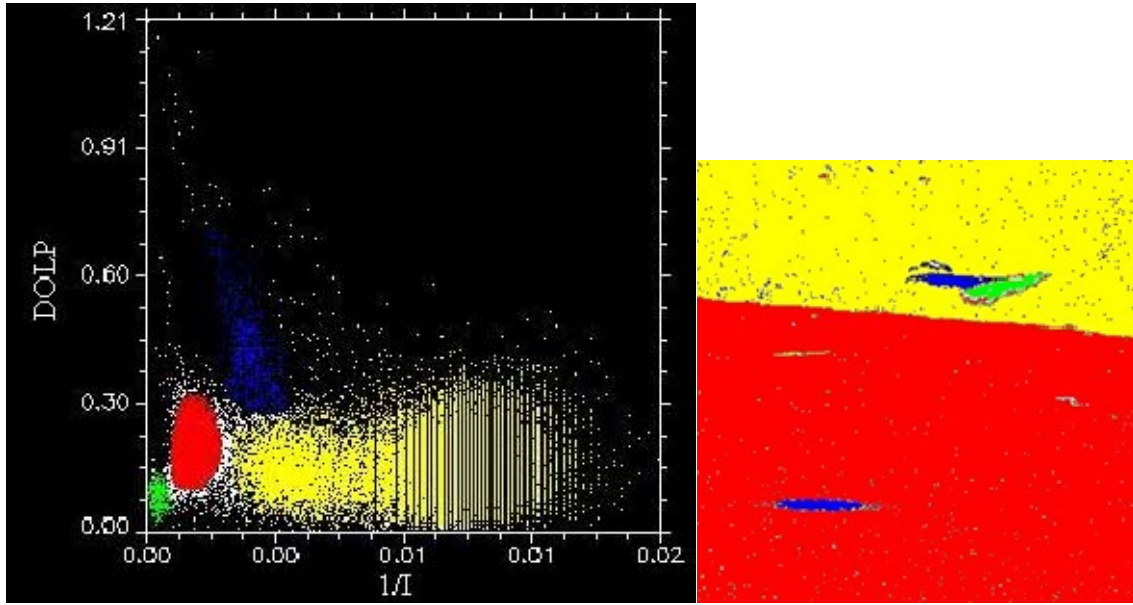
Figure 33.   Dug/Replaced Scatter Plot and Classification.

C.   UMOV EFFECT

To address the question of whether additional information is carried in DOLP, DOLP was scatter-plotted against the inverse of intensity for the dug/replaced patch and head-on sandbox images (see Figs. 33 and 34). Reflection from various surfaces appears in groupings in these plots, and these groupings were chosen as classes.

Based on the Umov effect, the expectation was to find a direct relationship between DOLP and inverse intensity when looking at various surfaces. This clearly occurs in the dug/replaced image (Fig. 33), where the brightest object (apparently a rock, colored green) has lowest polarization and is followed by the aged road surface (red) and the dark dug/replaced patch (blue) in a trend of decreasing intensity and increasing DOLP. In the chosen classification, the dug/replaced patch appears similar to a darker rock face. For completeness, the remainder of the scene is classified together (yellow).

In the sandbox image (Fig. 34), the Umov trend is less clear. The brightest classified surfaces are the rooftop (red) and cardboard (green), but contrary to the prediction of the Umov effect, they are more highly polarized than the darker sand (blue). On the other hand, the lower-albedo soil (yellow) is somewhat more highly polarized

47

than the sand, as expected. The filtered light was classified separately and appears very distinctly in the plot. The remaining unclassified groupings belong to various reflections from the plastic sandbox itself.

The discrepancy of the cardboard and rooftop with the Umov effect is likely due to the fact that the ground, cardboard, and soil/sand differ significantly as surface types. At least in the case of the fairly similar soil and sand, the Umov effect holds true. This observation also applies well to the dug/replaced asphalt, where the three surfaces that hold with the Umov effect—asphalt, upturned asphalt, and rock—are similar, at least in material makeup.

It is apparent from these plots that the Umov effect does hold, within limits. Therefore, there is a correlation between intensity and DOLP, but since the plots show differing distinctions in both quantities, it appears that the second interpretation in section V.B.4 above is more correct: intensity and DOLP convey different but partly correlated information. Notably, this correlation is broken by significant variations in surface material type.
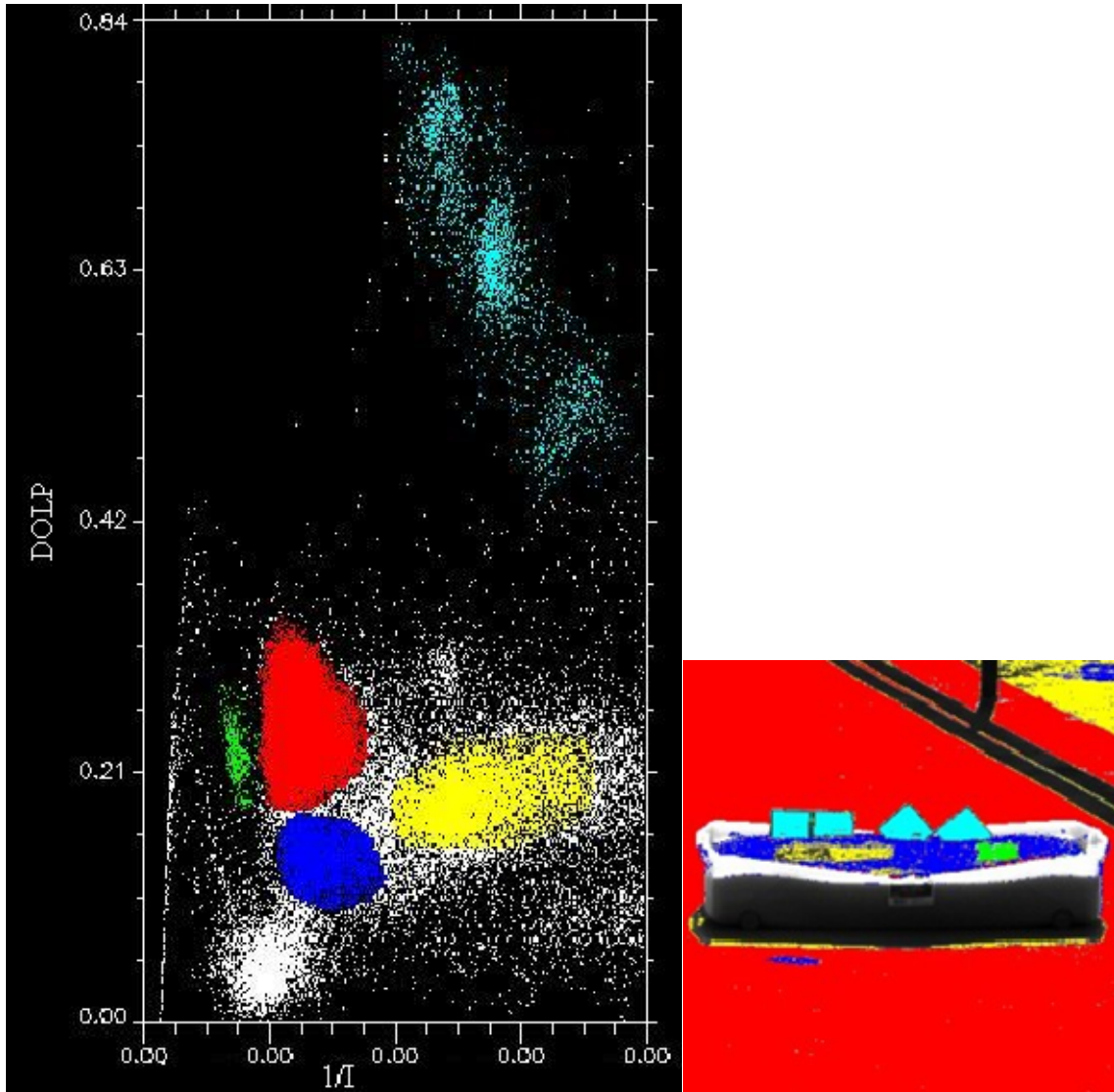
Figure 34.   Sandbox Scatter Plot and Classification.

THIS PAGE INTENTIONALLY LEFT BLANK

VI.   CONCLUSION

A.   SUMMARY OF OBSERVATIONS AND ANALYSIS

The SALSA polarimetric camera was tested for its disturbed-surface detection capability. Disturbed-earth detection was tested primarily by using a semi-controlled outdoor experiment looking at a sandbox filled with sections of sand, cardboard, and disturbed/undisturbed coarse sandy loam.   The resulting images were run through occurrence and co-occurrence texture filters, and region of interest separability was computed based on three of the co-occurrence measures.   The visible polarization difference of the disturbed and undisturbed earth was not particularly strong, though the earth was distinguishable from the surrounding sand. Separability measures agreed with these visual assessments.

Disturbed asphalt detection was tested by imaging two patchy parking lots, a patched neighborhood street, and a dug and replaced patch of asphalt in an old road surface. The camera showed a stronger ability to distinguish aged asphalt from newer asphalt, or the replaced asphalt from the surrounding road surface, than it did with disturbed and undisturbed earth. Maximum likelihood analysis performed on DOLP images yielded good results when classifying older against newer asphalt regions.

## B.   EVALUATION & RECOMMENDATIONS

1.   Assessment
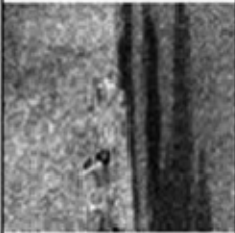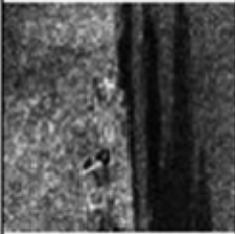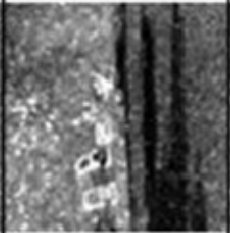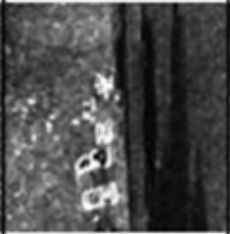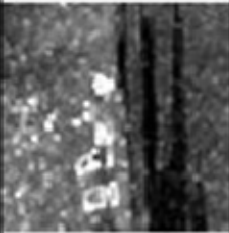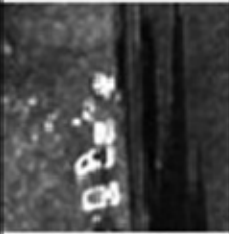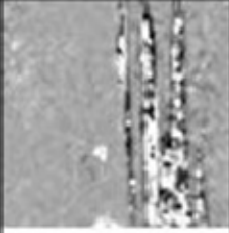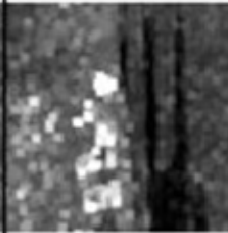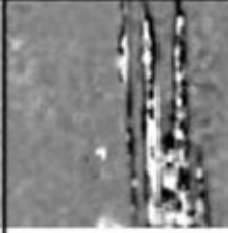
Two possible causes of the mediocre soil test results are a lack of sensitivity at green wavelengths to the soil surface roughness scale and dependence on the soil type employed. Both of these factors should be tested in further research. Based on the current results alone, the polarimetric camera does not show particular promise for augmenting visual search for IEDs buried under soil, but this judgment could be changed based on future investigations.

The more successful asphalt tests show some promise, though more investigation needs to be done to determine how much information is truly being provided by polarization. As previously stated, the polarization camera is truly useful only when differences are not already apparent in intensity. Therefore, the time interval during which relatively new patching is not visually obvious would be where polarimetric imaging would be most useful. To address this and to show that polarization effects (rather than an intensity inversion) are providing distinction in DOLP, more imaging should be performed on patches that appear similar to their surroundings in intensity.
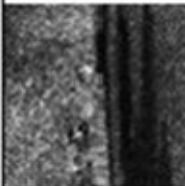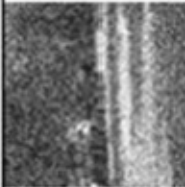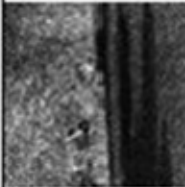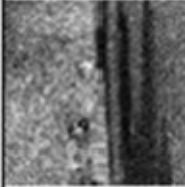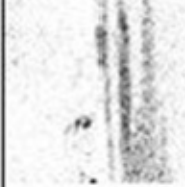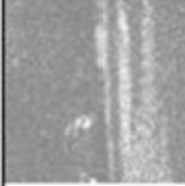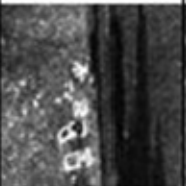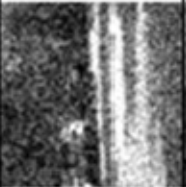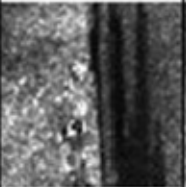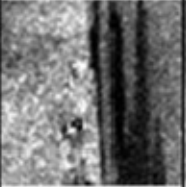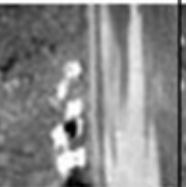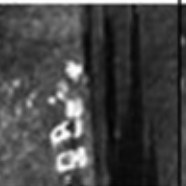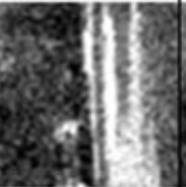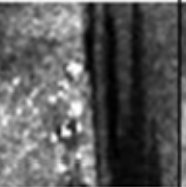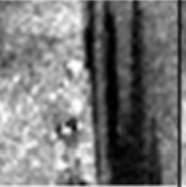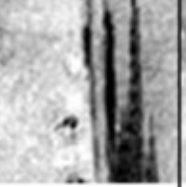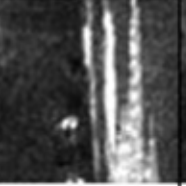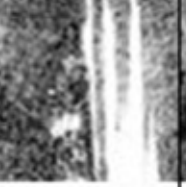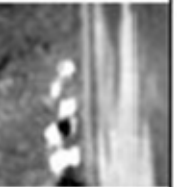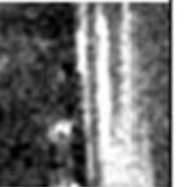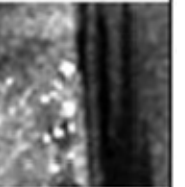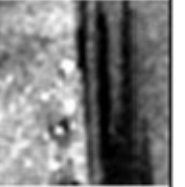
2.   Conclusion & Recommendations
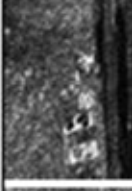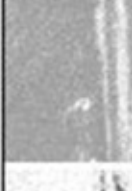
This research succeeded in making an initial evaluation of the SALSA camera's disturbed-surface detection capability. While disturbed-earth detection is relatively unpromising even when image processing is employed, it may prove more useful when looking at other soil types, observation wavelengths, or roughness scales. Asphalt imaging proved more useful, though further testing is required to assess the contribution of polarization to the observed DOLP signature of asphalt patches. In spite of disappointing initial results, this research did succeed in its secondary objective of providing some new polarization difference observations in a field where there is relatively little public data available.
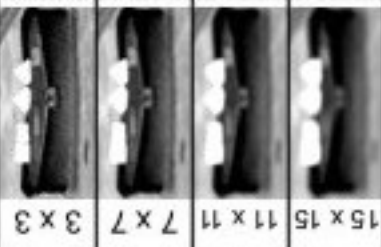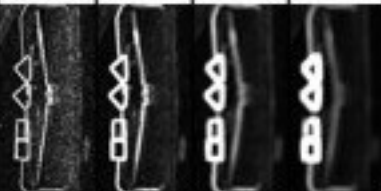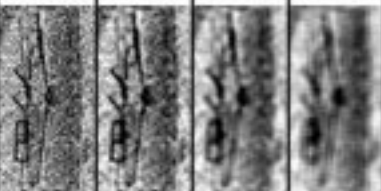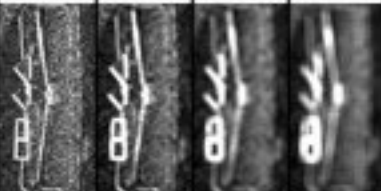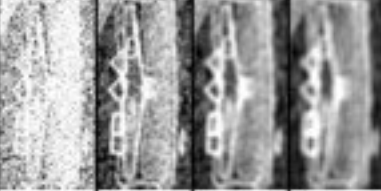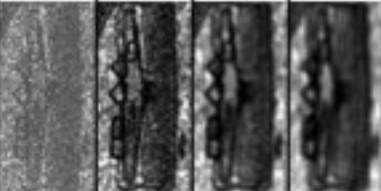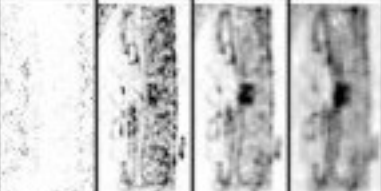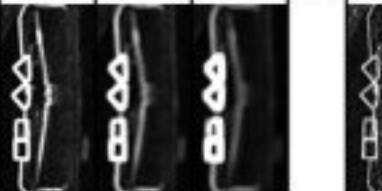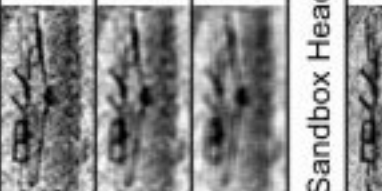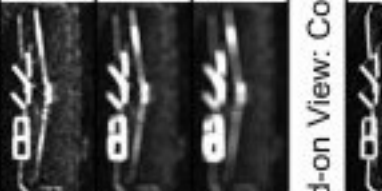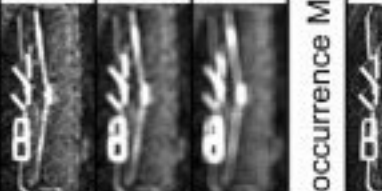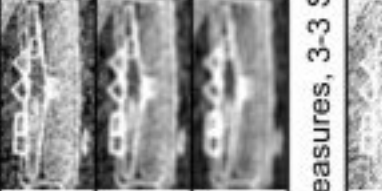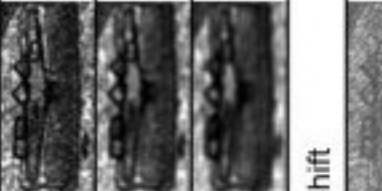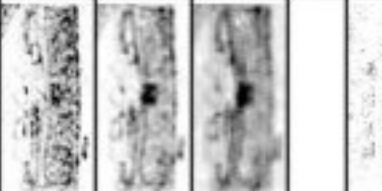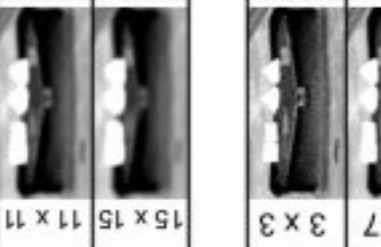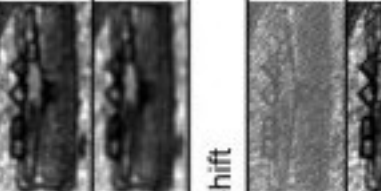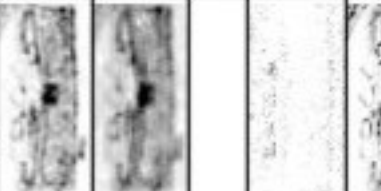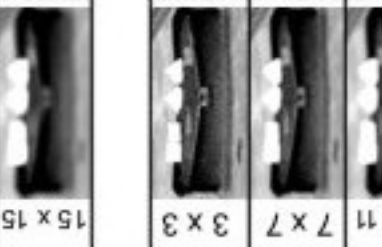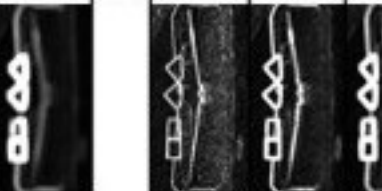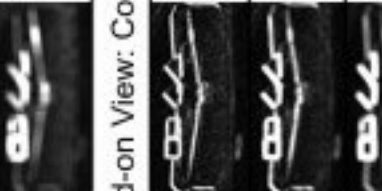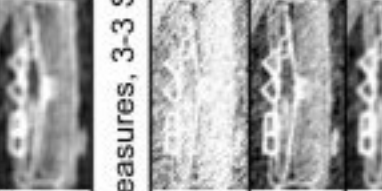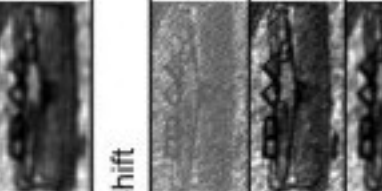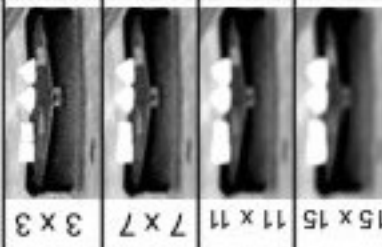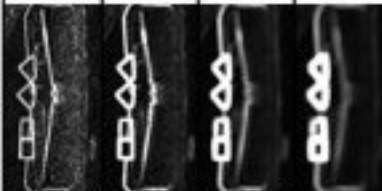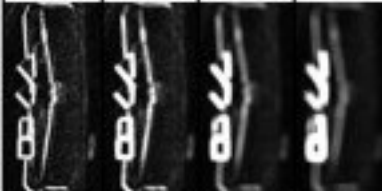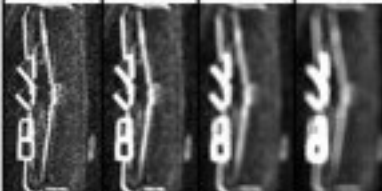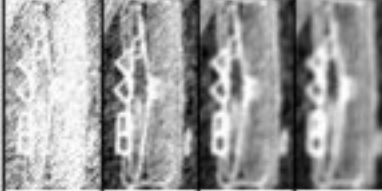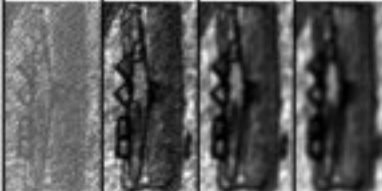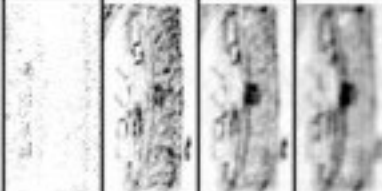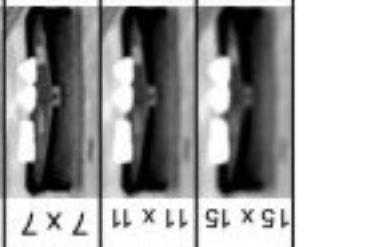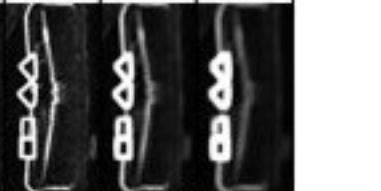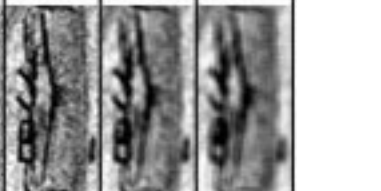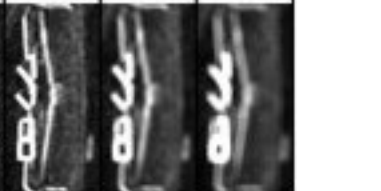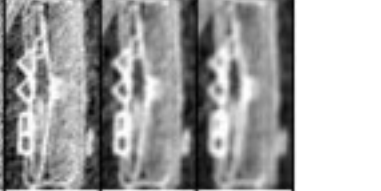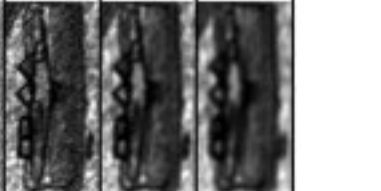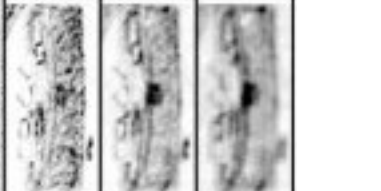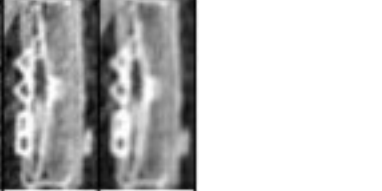
APPENDIX

S Lot: Occurrence Measures

Sandbox Occurrence Measures

	Mean	Data Range	Variance	Entropy	Skewness

Head-on View: 3 × 3, 7 × 7, 11 × 11, 15 × 15
Offset View: 3 × 3, 7 × 7, 11 × 11, 15 × 15

54

S Lot: Co-occurrence Measures, 1-1 Shift

S Lot: Co-occurrence Measures, 3-3 Shift

	Mean	Variance	Homogeneity	Contrast	Dissimilarity	Entropy	2nd Moment	Correlation
3×3								
7×7								
11×11								
15×15								

Sandbox Head-on View: Co-occurrence Measures, 1-1 Shift

Sandbox Head-on View: Co-occurrence Measures, 3-3 Shift

THIS PAGE INTENTIONALLY LEFT BLANK

LIST OF REFERENCES

Andreou, A. G., & Kalayjian, Z. K. (2002). Polarization imaging: Principles and integrated polarimeters. *IEEE Sensors Journal, 2*(4), 566-576.

Born, M., & Wolf, E. (1999). *Principles of optics : Electromagnetic theory of propagation, interference and diffraction of light* (7th expanded ed.). Cambridge; New York: Cambridge University Press.

Brewster, D. (1815). On the laws which regulate the polarisation of light by reflexion from transparent bodies. *Philos. Trans. R. Soc. London, 105*, 125-130, 158-159.

Collett, E. (2005). *Field guide to polarization (SPIE vol. FG05)* SPIE Publications.

Curran, P. J. (1978). A photographic method for the recording of polarised visible light for soil surface moisture indications. *Remote Sensing of Environment, 7*, 305-322.

Dollfus, A. (1998). Lunar surface imaging polarimetry: I. roughness and grain size. *Icarus, 136*, 69-103.

Egan, W. G., & Hallock, H. B. (1966). Polarimetry signature of terrestrial and planetary materials. *Proceedings of the 4th Symposium on Remote Sensing of Environment,* Infrared Physics Laboratory, University of Michigan, Ann Arbor. 671-689.

Egan, W. G., Grusauskas, J., & Hallock, H. B. (1968). Optical depolarization properties of surfaces illuminated by coherent light. *Applied Optics, 7*(8), 1529-1534.

Egan, W. G., Johnson, W. R., & Whitehead, V. S. (1991). Terrestrial polarization imagery obtained from the space shuttle: Characterization and interpretation. *Applied Optics, 30*(4), 435-442.

Egan, W., G., & Hallock, H. B. (1969). Coherence-polarization phenomena in remote sensing. *Proceedings of the IEEE, 37*(4), 621-628.

Egan, W. G. (1985). *Photometry and polarization in remote sensing*. New York: Elsevier.

Fung, A. K. (1966). Scattering and depolarization of EM waves from a rough surface. *Proceedings of the IEEE, 54*(3), 395-396.

Geake, J. E., Dollfus, A., Garlick, G., Lamb, W., Walker, G., Steigmann, G., et al. (1970). Luminescence, electron paramagnetic resonance and optical properties of lunar material from apollo 11. *Apollo 11 Lunar Science Conference 3rd,* 2127-2147.

Haralick, R. M., Shanmugam, K., & Dinstein, I. (1973). Textural features for image classification. *IEEE Transactions on Systems, Man, and Cybernetics, SMC-3*(6), 610-621.

Humphrey, M. D. (2003). Texture analysis of high resolution panchromatic imagery for terrain classification. (M.S. in Applied Physics, Naval Postgraduate School), 131. (Springfield, Va. : Available from National Technical Information Service)

iCasualties.org: Iraq coalition casualty count. (2009). Retrieved May 2009, from http://icasualties.org/

JIEDDO. (2009). *JIEDDO overview, history, and objectives.* Retrieved February 2009, from https://www.jieddo.dod.mil/ABOUTJIEDDO/AJHOME.ASPX

Können, G. P. (1985). *Polarized light in nature*. Cambridge, Cambridgeshire; New York: Cambridge University Press.

Lefaudeux, N., Lechocinski, N., Breugnot, S., & Clemenceau, P. (2008). Compact and robust linear stokes polarization camera. *Proceedings of the SPIE, , 6972* 69720B-69720B-12.

Malus, M. (1809). Sur une propriété de la lumière réfléchie. *Mém. Phys. Chim. Soc. d'Arcueil, 2*, 143-158.

Olsen, R. C. (2007). *Remote sensing from air and space*. Bellingham, Wash: SPIE Press.

Puetz, A. M., & Olsen, R. C. (2006). Haralick texture features expanded into the spectral domain. *, 6233*(1) 623311.

Rees, G. (2001). *Physical principles of remote sensing* (2nd ed.). Cambridge, U.K; New York, NY: Cambridge University Press.

Richards, J. A., & Jia, X. (1999). *Remote sensing digital image analysis : An introduction* (3rd ed.). Berlin; New York: Springer.

Secchi, P. A. (159). Letter from Father Secchi to the Astronomer Royal on the polarisation of light reflected by the moon. *Monthly Notices of the Royal Astronomical Society, 19*(8), 289.

Stokes, G. G. (1852). On the composition and resolution of streams of polarized light from different sources. *Transactions of the Cambridge Philosophical Society, 9*, 399-416.

Talmadge, D. A., & Curran, P. J. (1986). Remote sensing using partially polarized light. *International Journal of Remote Sensing, 7*(1), 47-64.

Tyo, J. S., Goldstein, D. L., Chenault, D. B., & Shaw, J. A. (2006). Review of passive imaging polarimetry for remote sensing applications. *Applied Optics, 45*(22), 5453-5469.

Valenzuela, G. (1967). Depolarization of EM waves by slightly rough surfaces. *IEEE Transactions on Antennas and Propagation, 15*(4), 552-557.

Wolinski, T. R. (2003). Polarization phenomena in optical systems. In R. G. Driggers (Ed.), *Encyclopedia of optical engineering* (pp. 2150-2173) CRC Press.

Zorpette, G. (2008). Countering IEDs. *IEEE Spectrum, 45*(9), 26-35.

THIS PAGE INTENTIONALLY LEFT BLANK

INITIAL DISTRIBUTION LIST

1. Defense Technical Information Center
   Ft. Belvoir, VA

2. Dudley Knox Library
   Naval Postgraduate School
   Monterey, CA

3. Dr. Richard C. Olsen, Code PH
   Naval Postgraduate School
   Monterey, CA

4. Nicolas Lefaudeux.
   Bossa Nova Technologies, LLC
   Venice, CA